

Towards improved cover glasses for photovoltaic devices

ALLSOPP, Ben, ORMAN, Robin, JOHNSON, Simon, BAISTOW, Ian, SANDERSON, Gavin, SUNDBERG, Peter, STALHANDSKE, Christina, GRUND, Lina, ANDERSSON, Anne, BOOTH, Jonathan, BINGHAM, Paul <<http://orcid.org/0000-0001-6017-0798>> and KARLSSON, Stefan

Available from Sheffield Hallam University Research Archive (SHURA) at:

<https://shura.shu.ac.uk/26854/>

This document is the Published Version [VoR]

Citation:








ALLSOPP, Ben, ORMAN, Robin, JOHNSON, Simon, BAISTOW, Ian, SANDERSON, Gavin, SUNDBERG, Peter, STALHANDSKE, Christina, GRUND, Lina, ANDERSSON, Anne, BOOTH, Jonathan, BINGHAM, Paul and KARLSSON, Stefan (2020). Towards improved cover glasses for photovoltaic devices. Progress in Photovoltaics: research and applications. [Article]

Copyright and re-use policy

See <http://shura.shu.ac.uk/information.html>

RESEARCH ARTICLE

Towards improved cover glasses for photovoltaic devices

Benjamin L. Allsopp¹  | Robin Orman² | Simon R. Johnson² | Ian Baistow³ |
Gavin Sanderson³ | Peter Sundberg⁴  | Christina Stålhandske⁴  |
Lina Grund⁴  | Anne Andersson⁵  | Jonathan Booth² | Paul A. Bingham¹  |
Stefan Karlsson⁴ 

¹Materials and Engineering Research Institute, Sheffield Hallam University, City Campus, Howard Street, Sheffield, S1 1WB, UK

²Catalyst and Materials Department, Johnson Matthey Technology Centre, Blounts Court, Sonning Common, Reading, RG4 9NH, UK

³PV Technology Centre, Solar Capture Technologies, Albert Street, Blyth, NE24 1LZ, UK

⁴Built Environment Division, Glass Section, RISE Research Institutes of Sweden, Växjö, SE-351 96, Sweden

⁵Safety and Transport Division, Time and Optics Section, RISE Research Institutes of Sweden, P.O. Box 857, Borås, SE-501 15, Sweden

Correspondence

Stefan Karlsson, Built Environment Division, Glass Section, RISE Research Institutes of Sweden, Växjö SE-351 96, Sweden.
Email: stefan.karlsson@ri.se

Paul A. Bingham, Materials and Engineering Research Institute, Sheffield Hallam University, City Campus, Howard Street, S1 1WB, UK
Email: P.A.Bingham@shu.ac.uk

Funding information

Swedish Energy Agency, Grant/Award Number: 38349-1; Technology Strategy Board, Grant/Award Number: 620087; Solar-ERA, NET, Grant/Award Number: 005

Abstract

For the solar energy industry to increase its competitiveness, there is a global drive to lower the cost of solar-generated electricity. Photovoltaic (PV) module assembly is material-demanding, and the cover glass constitutes a significant proportion of the cost. Currently, 3-mm-thick glass is the predominant cover material for PV modules, accounting for 10%–25% of the total cost. Here, we review the state-of-the-art of cover glasses for PV modules and present our recent results for improvement of the glass. These improvements were demonstrated in terms of mechanical, chemical and optical properties by optimizing the glass composition, including addition of novel dopants, to produce cover glasses that can provide (i) enhanced UV protection of polymeric PV module components, potentially increasing module service lifetimes; (ii) re-emission of a proportion of the absorbed UV photon energy as visible photons capable of being absorbed by the solar cells, thereby increasing PV module efficiencies and (iii) successful laboratory-scale demonstration of proof of concept, with increases of 1%–6% in I_{sc} and 1%–8% in I_{pm} . Improvements in both chemical and crack resistance of the cover glass were also achieved through modest chemical reformulation, highlighting what may be achievable within existing manufacturing technology constraints.

KEYWORDS

chemical properties, cover glass, mechanical properties, optical properties, photoluminescence, PV modules, strengthening of glass

1 | INTRODUCTION

Solar energy is often seen as the ultimate renewable energy because of the abundance of solar irradiation available for solar energy generation. In only 90 min, the Earth receives enough energy from the sun to provide its entire annual energy requirements.¹ Chapin, Fuller and Pearson invented the first practical photovoltaic (PV) cell in 1954,²

and since the year 2000, installed PV capacity has experienced an almost exponential growth.³ The installed PV capacity can be regulated politically but that is largely achieved on a national level and may be subject to change within just a few years. The growth of the solar energy market has been driven by the reduction of costs. For solar or any other renewable energy source, it has been a necessity to compete on an economical level (i.e., reaching so-called grid parity), and

This is an open access article under the terms of the Creative Commons Attribution License, which permits use, distribution and reproduction in any medium, provided the original work is properly cited.

© 2020 The Authors. Progress in Photovoltaics: Research and Applications published by John Wiley & Sons Ltd

thereby renewable energy has now become a real competitor to non-renewable energy sources. Grid parity has been achieved by several countries,^{4,5} for example, Japan, Australia, Germany, Italy, Greece, Turkey, Spain and Argentina. The comparison of costs for different energy sources is known as the 'levelized cost of electricity' (LCOE) and provides a good benchmark to different energy sources.⁶ The LCOE for PV energy has decreased rapidly in the last 10 years and is now competitive, in the range of US\$32–42/MWh.⁷

In the PV industry, the measure of the direct current peak power rating (W_p) is a conventional benchmark among PV modules, which reflects the system efficiency under standardized conditions.⁸ The cost, expressed as either LCOE or cost per Watt peak (W_p), is a driving factor for maintaining the exponential trend for installed PV capacity.⁹ As shown in Ray,⁷ the LCOE reduction has flattened out and so has the cost per W_p ; therefore, the PV industry and market need new innovations to further reduce costs. The reduction of costs will primarily be achieved by (i) increasing solar device efficiency, (ii) reducing balance of system costs and (iii) minimizing the module cost. The properties of PV module materials are of great importance to ensure optimal light capture and module lifetime as well as ultimately reducing the cost.⁹ Although these figures are a few years old, they provide a useful guide to the importance of the fractional cost of cover glass within PV modules. The cover glass constitutes about 25% of the cost of Si thin-film modules¹⁰ and about 10%–15% of the cost of crystalline Si (c-Si) modules¹¹ as compared with the grid-parity aim (US \$0.5–0.7/ W_p). At the time of writing, the spot market price is about US\$0.3/ W_p for polycrystalline-Si and slightly lower for mono-Si modules⁹; thus, the glass fractional cost is increasing as the cost per W_p is decreasing. Improving the cover glass and reducing its cost thus become increasingly important, and the three main approaches for reducing material costs are identified as (i) reducing material thickness, (ii) replacing expensive raw materials and (iii) reducing material waste.⁹ The market share from the PV energy industry in global flat glass production was less than 2% in 2015, but the growth of installed PV capacity increases annually, with prognoses even claiming that the PV industry will demand an expansion of global flat glass production in the near future.^{8,10,12} The global flat glass industry thus has rapidly growing interest in this field.¹⁰

Today, mono- and poly-crystalline Si solar cells dominate the PV market, balancing the state of the art and economy; see Figure 1 for the Shockley–Queisser theoretical limit as a function of bandgap wavelength.¹³ The costliest module components are the active semiconductor material (Si) and the glass cover. Typical dimensions of a domestic PV module are 1.4–1.7 m², with >90% covered by soda-lime-silica (SLS) float glass.⁹ The glass alone weighs ~20–25 kg since the density of SLS glass is ~2520 kg/m³. This presents engineering challenges as current solar panels are rigid and need strong, heavy support structures. Rigidity and weight confine exploitation of portable PV products, and the production of high volumes of glass carries both energy and environmental costs, contributing to global CO₂ emissions. Service lifetimes and efficiencies of solar cell components are limited by solar UV radiation damage, which induces degradation of laminate materials, the most frequently used being ethylene vinyl

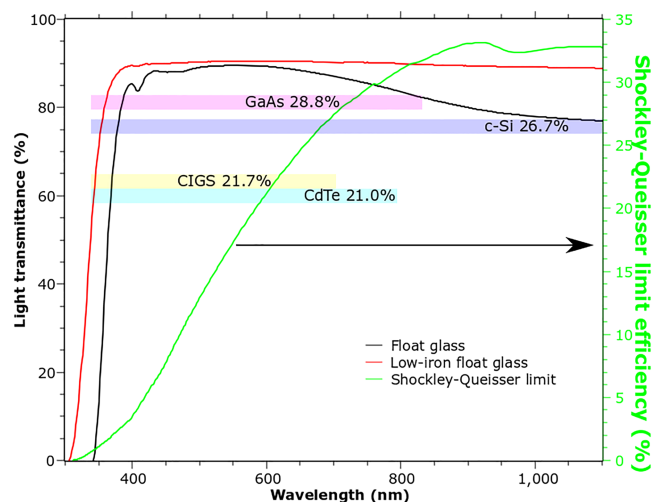


FIGURE 1 Left y-axis shows UV–Vis–nIR transmission spectra of conventional float glass and low-iron float glass (4-mm thickness) as a function of wavelength. Right y-axis shows the Shockley–Queisser theoretical limit as a function of semiconductor bandgap wavelength, with data adapted from Rühle.¹³ Insets show the absorption onset of some semiconductors used in commercial single-junction PV modules with achieved efficiencies according to¹⁴ (1) GaAs (gallium arsenide thin films), (2) c-Si (crystalline silicon both as wafers and thin films), (3) CIGS (copper indium gallium selenide) and (4) CdTe (cadmium telluride thin films)⁸ [Colour figure can be viewed at wileyonlinelibrary.com]

acetate (EVA), eventually leading to delamination and module failure,¹⁵ although in recent years, 'transparent EVA' or T-EVA, with a UV cut-off wavelength of ~300 nm, has been developed,¹⁶ reducing this effect. However, discolouration and delamination of T-EVA can still arise at the backsheet interface in PV modules, as recently discussed by Adothu et al.¹⁷ They also demonstrated discolouration and photobleaching of T-EVA in c-Si PV module tests, with yellowness indices, following UV exposure, that were approximately one-quarter those of traditional UV-cutting EVA (C-EVA).¹⁷ Although a significant improvement, the yellowness index of the T-EVA was still nonzero. Moreover, the environmental stability of the T-EVA encapsulant is still not known.¹⁷ Consequently, although T-EVA represents an important step forward and enables increases in PV module efficiency by comparison with C-EVA,¹⁷ T-EVA does not necessarily present a panacea for environmental degradation of PV module encapsulants. Undoubtedly, there remains room for further improvement.

There is a genuine and growing need to reduce the thickness (= weight) of the glass cover while improving PV module service lifetimes and efficiencies. Today, commercial 3-mm-thick toughened PV glass provides only limited benefits: Low-iron content is used to improve solar transmittance¹⁸; see Figure 1. The Fe²⁺/Fe³⁺ redox ratio in the glass may be controlled through the use of oxidizing agents in glass raw materials mixtures (batches), providing a degree of chemical decolourization.^{19,20} Also, the glass surface may be patterned^{21,22} or coated²³ so that some light can be guided back towards the solar cell, or to reduce reflection losses at glass-air interfaces via antireflective (AR) coatings.²⁴ Even small increases in solar light

transmission through the cover glass can have a significant commercial advantage, for example, a 5% increase in solar transmittance could result in up to 10% improvement in energy collection efficiency.²⁵ Here, we review the current state of the art for optical and mechanical properties of PV module cover glasses, and we present research on how development of the cover glass composition, and the use of novel dopants therein, may provide pathways to improve the efficiency, service lifetime and weight of PV modules, in addition to providing a perspective on the challenges that remain.

1.1 | Optical properties of cover glasses for PV applications

Current commercial float glasses transmit ~90% of incident light, with the primary sources of loss being absorption and reflection. If the glass is AR-coated, it is possible to achieve ~98% light transmission. Here, we focus on the bulk glass material itself, and coatings or nanopatterning are beyond the scope. For an introduction to AR coatings, the reader is referred to Deubener et al.²¹ and for nanopatterned glass to Gombert et al.²⁶ Cover glass can be sensitive to corrosive media (e.g., acid rain) and water,^{27,28} and low-iron cover glass has only limited capability to block the UV radiation that damages both the active semiconductor materials²⁹ and the EVA laminate¹⁵ within a PV module, with the latter being the dominating degradation mechanism. However, as noted in Section 1, recent developments on EVA laminate chemistry to develop T-EVA have rendered EVA partly transparent to UV with a cut-off wavelength of ~300 nm,¹⁶ which is approximately the same wavelength as the UV cut-off for low-iron glass (c.f. Figure 1). Despite the availability and recent application of these new EVA materials (see, e.g., Vogt et al.¹⁶ and Adothu et al.¹⁷), they remain susceptible to UV- and temperature-induced discolouration and delamination (see Section 1), and it remains important to have an appropriate level of UV blocking, otherwise degradation of the laminate is a major limiting factor of the service lifetime and lifetime efficiency of PV modules. For traditional C-EVA, this could lead to annual degradation of 0.6%–2.5% in PV module efficiency because of degradation of the C-EVA, depending on service conditions and manufacturer.^{15,30,31} The main effect is discolouration of the EVA layer due to UV damage, resulting in reduced light transmission and thus contributing to reduced module efficiency.³² The mechanisms and chemical species involved in this discolouration were recently summarized by Adothu et al.¹⁷ In addition to its effects on the polymeric encapsulant materials, UV degradation can also impact on the efficiency of the solar cell material itself. This was demonstrated by Shamachurn and Betts,³³ who observed deterioration of solar cell efficiency for bare Si solar cells, which they attributed in part to degradation of the antireflective coating on the cell material. This further underlines the need for an appropriate level of UV protection for PV module materials, ideally provided by the first 'barrier', that is, the glass cover sheet.

The incorporation of small quantities of iron oxide (Fe_2O_3) into the SLS cover glass shifts the UV absorption edge strongly towards

longer (visible) wavelengths. This arises because of strong oxygen-metal charge transfer (OMCT) bands centred in the deep UV, which exhibit tails to longer wavelengths,³⁴ and also characteristic absorption bands between ~360 and ~460 nm arising from $d-d$ transitions of Fe^{3+} ions.³⁴ Both Fe^{3+} and Fe^{2+} ions typically occur in commercially manufactured float glass, and the presence of Fe^{2+} parasitically absorbs photons within the nIR and red-visible region with a strong, broad absorption band centred at approximately 1000 nm,³⁴ which particularly affects the efficiency of Si PV modules. Even low quantities of Fe_2O_3 (e.g., 0.01 mol%) in SLS glass result in a loss in PV module output power of 1.1% and with 0.10-mol% Fe_2O_3 present in the glass, this results in a 9.8% loss.³⁵ However, although minimizing the Fe_2O_3 content of the glass provides obvious improvements in PV efficiency, it reduces the protection against UV degradation afforded to the other PV module components. This presents engineers with somewhat of a dilemma—balancing the need to improve efficiencies in the short term while maintaining module efficiencies and service lifetimes in the longer term. A combination of reducing the concentration of iron oxide species within the glass front sheet, while providing sufficient absorption of UV photons to protect the EVA and/or other polymeric species, is thus of paramount importance for developing more efficient and longer lasting PV modules.

A suggested solution has been to dope the low-Fe glass with active optical centres that, unlike Fe, do not produce visible or nIR absorption bands, but do absorb UV photons and, moreover, re-emit a proportion of the absorbed energy as photons of visible light. This process is frequently called down-conversion or down-shifting, depending on the type of electronic transition involved (see Figure 2).^{36,37} This aspect of photoluminescence has been considered since the 1970s^{38–41} and is still receiving attention.^{37,42,43} By using down-conversion^{44,45} or down-shifting, the solution is two-fold as the doped glass both absorbs harmful UV photons but also re-emits some of this absorbed energy as photons of visible light that can be captured and converted by the solar cell. Thus, it can increase the PV module service lifetime while enhancing the module efficiency. Fluorescent glasses have been widely studied and most lanthanide-containing glasses fluoresce at visible wavelengths.⁴⁶ A detailed treatment of the use of different lanthanide cations as spectral converters for PV cells was provided by van der Ende et al.⁴⁷ The fluorescent components can either be doped directly into the bulk glass during manufacture, or they can be applied as coatings on the surface of the glass using post-processing steps such as sol-gel,^{48,49} spray-pyrolysis⁵⁰ or nanoparticles⁵¹ via ion exchange.^{52,53} Luminescent materials have also been considered for use in solar collector concentrators⁵⁴ where the light can be wave guided (by internal total reflection) to the sides of a window where solar cells are located.^{55,56}

Selection of glass dopant cations that produce no absorption bands at visible or near-IR energies is essential, otherwise any benefits for UV protection are likely to be outweighed by the negative impact on light transmission of the cover glass and thus solar cell efficiencies. The large majority of first-row transition metals, when doped into glasses, suffer this limitation.^{34,35,57–60} Other metal ions can also absorb UV photons and provide down-shifted or down-converted

fluorescence at visible wavelengths and recently Bi³⁺-doped glasses have been suggested as promising materials for solar spectral conversion.^{61,62} Ion incorporation of Cu⁺ by exchange has also shown promise.⁵² In addition, recent research by some of the present authors^{63,64} has demonstrated that a number of second- and third-row transition metal dopants which adopt the d^0 electronic configuration in glasses (Ti⁴⁺, Zr⁴⁺, Hf⁴⁺, Nb⁵⁺, Ta⁵⁺, Mo⁶⁺ and W⁶⁺),⁶³ and also heavy metal cations such as Sb which exhibit far-UV absorption bands from $s \rightarrow p$ electronic transitions⁶⁵ can also provide down-shifting of UV photons in silicate glasses with negligible visible absorption.⁶³ Moreover, some of the present authors have also shown that adding Gd³⁺ or other lanthanides as a co-dopant with Bi³⁺ can provide enhanced luminescence intensity compared with Bi³⁺ doping alone.⁶⁴

In terms of luminescence mechanisms, down-conversion and down-shifting from UV to visible wavelengths have been the most commonly studied approaches, but up-conversion^{37,66} from the IR range to visible wavelengths is also an alternative; see Figure 2. Up-conversion^{37,67,68} could also provide benefits in terms of enhanced solar cell efficiency, as most solar cells decrease in efficiency with increased temperature; therefore, up-converting glass constituents could absorb IR photons and moderate solar cell temperature, in addition to the benefit of providing more nIR and visible light with energy greater than the semiconductor bandgap energy available for conversion by the solar cell. Dopants responsible for producing up-conversion in glasses have typically been lanthanides (see, e.g., Dejneka et al⁴⁶). However, the conversion efficiency of up-conversion in glasses is low, even in exotic glass chemistries that are greatly different to commercial SLS glasses and unsuited to low-cost,

high-volume manufacture. Furthermore, the majority of studies of up-conversion in glasses have relied on laser light sources to enable measurable levels of up-conversion. Development of new low-cost silicate glasses with economically viable up-conversion with sufficient efficiency improvements remains a considerable research challenge.

Given the above evidence, in this study, we have focused on the development of new down-shifting glass formulations, with selection of nontoxic Bi³⁺ coupled with Gd³⁺ as dopants for further development and testing in lab-scale PV modules. Research considering other dopants capable of providing combinations of down-shifting, down-converting and up-converting mechanisms including, but not limited to those dopants listed above, is planned for future research.

1.2 | Mechanical performance of glass for PV applications

In addition to optical and environmental performance, the mechanical performance of PV modules is also of vital importance, and with the glass front sheet constituting a high proportion of the mass of PV modules, it also impacts on mechanical properties of the PV module composite. Consequently, it is important to develop new glasses with enhanced or improved strengths and toughness's compared with existing glasses, particularly in light of the drive towards thinner glasses to reduce weight and costs (see Section 1). The strength of glass is an extrinsic property that depends to a major extent on the surface of the glass rather than of the bulk glass.⁶⁹ In the linear elastic fracture mechanics theory, that brittle materials obeys, the critical stress intensity factor (K_{Ic}), which is a material property⁷⁰ for when a material fractures ($K_I \geq K_{Ic}$ = Fracture Toughness), where K_I is the stress intensity factor. By prestressing the glass surface with residual compressive stresses, it is possible to increase the fracture toughness by the failure criterion $K_{Ic} + K_{rs}$.⁷¹

Thermal toughening of PV cover glass is the most conventional route to meet the standard IEC 61215 on impact resistance that is aimed to simulate hailstorms. In this process, the glass is rapidly quenched with dry or humid pressurized air from temperatures $\sim 75^\circ\text{C}$ above the glass transition temperature (T_g).⁷² Initially, the glass surface starts to cool and contract more rapidly than the interior; the interior will be in compression, whereas the surface is in tension. At T_g , the glass surface becomes an elastic solid, whereas the hotter interior still is a viscoelastic body that can undergo structural and stress relaxation.⁷³ As the glass continues to cool, the glass surface will contract much less than the interior, and the glass surface will therefore be placed in a state of compression while the interior develops balancing tensile stresses. The residual stress profile is often of parabolic type (Figure 3A), and the central tensile stresses are approximately half the value of the compressive stresses at the surface.⁷⁵

In practice (Figure 4), the glass is cooled within a few tens of seconds from a temperature higher than 600°C to ambient temperatures. During the first few seconds, the temperature decreases at the

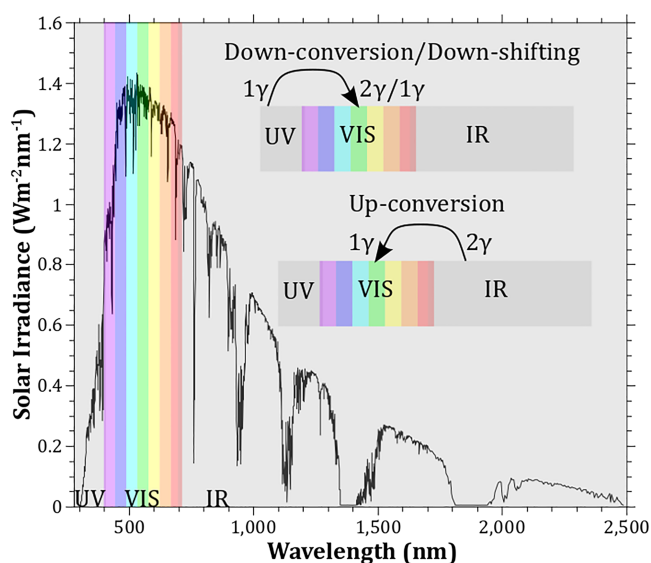
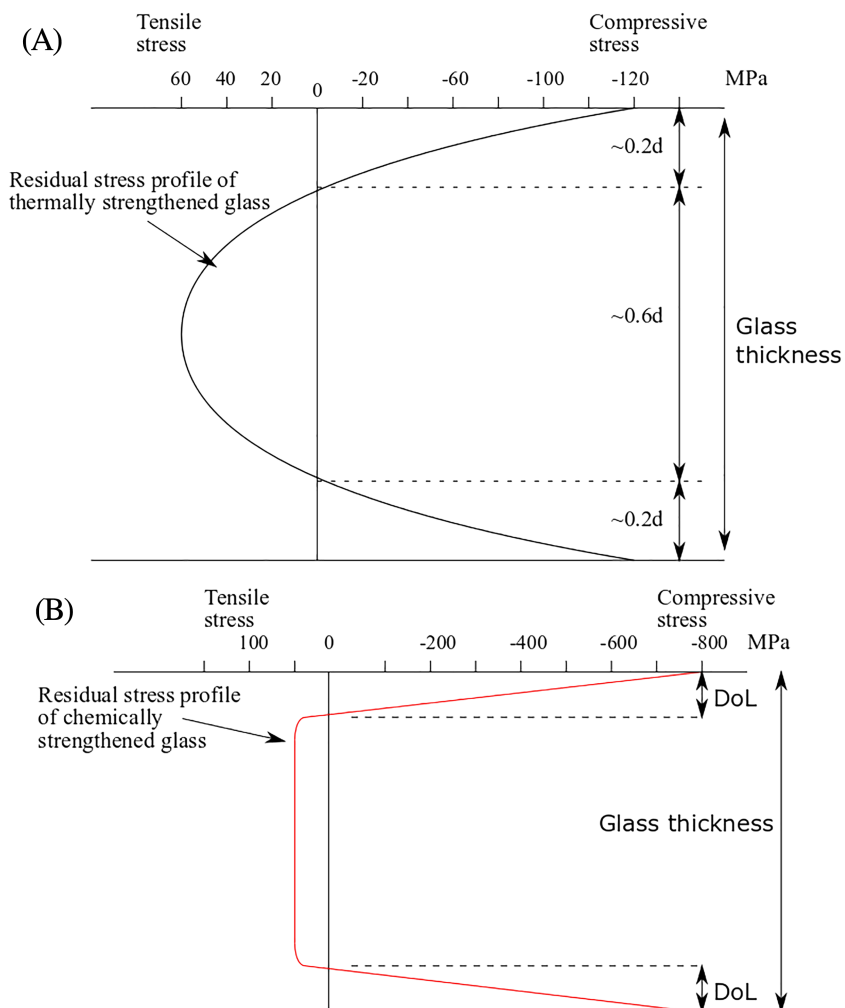


FIGURE 2 Solar irradiance spectra (black solid line) as a function of wavelength (nm) for air mass 1.5 according to ASTM-G173-03(2012). The insets demonstrate the principles of solar spectral adjustment: down-conversion ($1\gamma_{UV} \rightarrow 2\gamma_{VIS}$), down-shifting ($1\gamma_{UV} \rightarrow 1\gamma_{VIS}$) and up-conversion ($2\gamma_{IR} \rightarrow 1\gamma_{VIS}$) of light for increased harvest of solar energy [Colour figure can be viewed at wileyonlinelibrary.com]

FIGURE 3 Schematic overview of the residual stress profile of (A) thermally strengthened glass (soda–lime–silica glass) and (B) chemically strengthened glass (sodium–aluminosilicate glass)⁷⁴ [Colour figure can be viewed at wileyonlinelibrary.com]



surface by more than 150°C. Thermal strengthening depends greatly on the thermal expansion coefficient, α , of the glass and has been theoretically described by Narayanaswamy and Gardon.⁷³ Thus, not all glasses are suitable for thermal toughening, for example, glasses that have lower α do not thermally toughen well in practice, for example, Pyrex borosilicate glass ($\alpha \sim 3.3 \times 10^{-6} \text{ K}^{-1}$). Thermal toughening of glass depends not only on α but also on the quality of the parent glass and the maximum cooling rate that is practically achievable. SLS glass ($\alpha \sim 9 \times 10^{-6} \text{ K}^{-1}$) is the most commonly used glass in PV, as well as architectural applications (EN 572-2). Thermally toughened glass is also called *safety glass* because it fractures into small fragments, which are in general much less sharp and dangerous than the large dagger-like pieces of broken annealed glass. One drawback of thermally toughened glass is that it suffers from a spontaneous cracking problem as nickel sulphide (NiS) can be introduced into the glass as a contaminant from the raw materials. This is not a frequent occurrence, at most in 1 out of 500 glasses, and there is a method to eliminate this problem called the heat soak test.^{77,78} Nevertheless, a number of high-profile cases of spontaneous failure of architectural glass, which have ultimately been identified as originating from NiS inclusions, have been reported in the media.

Theoretically, the highest cooling rates enable the highest compressive stresses to develop in the glass surface and thus for thinner glass to be toughened. Upon too rapid cooling, however, the initial thermal gradient and surface tensile stresses can become so large as to cause glass fracture. The temporary tensile stresses that develop at the glass surface during cooling from the initial temperature (T_i) to T_g is described by Gulati et al.⁷⁹ With conventional cooling rates, the temporary tensile stresses are ~ 40 MPa. The residual stresses depend on the thickness of glass, the thinner glass; the greater cooling rates are needed to achieve same magnitude of residual stresses. Similarly, for a given thickness, the magnitude of the residual stresses is a function of the cooling rate. Therefore, it has previously been a critical limit of the thickness of the glass that can be thermally toughened by conventional processes. Traditionally, 3 mm was considered the minimum thickness, but with an improved process, 2 mm or thinner glass has recently been toughened. In this state-of-the-art process, the rollers are replaced by gas flotation systems in the furnace (e.g., the HZL technology of the LiSEC group and Glaston's GlastonAir™).⁷⁴ In this respect, eliminating the ceramic rollers is very important because they readily introduce surface defects onto the glass such as roller waves or scratches, thereby

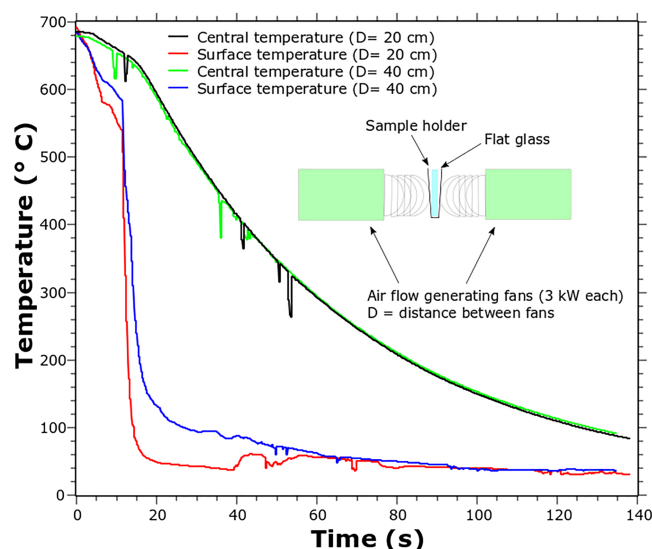


FIGURE 4 Measured temperatures during thermal tempering of glass by use of a thermocouple. Central temperature was measured in between two glass samples. The thermocouple was put in a carved slit in each of the glass sample. Upper curves represent the Centre temperature, that is, between the two glasses, at cooling and the lower curves represent the measured surface temperatures at different distance between cooling fans [Colour figure can be viewed at wileyonlinelibrary.com]

increasing the susceptibility to fracture, and they may also act as heat sinks during the quenching giving inhomogeneous toughening.

Another type of toughened glass that has received much interest recently is chemically toughened glass. This is based on thermally assisted ion exchange below T_g and involves incorporation of larger ions into the glass surfaces that induce compressive stresses. Compared with thermally toughened glass, higher compressive stresses can be achieved (Figure 3B) but at a considerably higher cost. Chemically toughened glass has found wide usage as cover materials for electronic devices but recently also in architectural and automotive applications.⁸⁰ Chemical toughening of glass has recently been extensively reviewed.^{75,81–84} The price of chemically toughened glass compared with thermally toughened glass is a factor of about two to six times. It has been used for more demanding PV applications such as space PV panels.⁸⁵ Recently, a chemically toughened cover glass for the PV industry, LeoFlex™, has been released.⁸⁶

Surface defects determine the strength of glass as given from the Griffith criterion for brittle materials.⁸⁷ Therefore, besides toughening, there are also other ways to increase the inherent toughness and strength of the glass,⁶⁹ for example, by increasing its resistance to scratches and cracks during handling. This has often been studied by indentation technology techniques.⁸⁸ Damage resistance of glasses has traditionally been described by the brittleness of glass,⁸⁹ which has often been described as the ratio of the hardness of the material and the indentation fracture toughness.⁹⁰ SLS glasses are optimized to a large extent based on the cost, melting and viscosity behaviour,

especially the float glass composition is optimized to suit the float process.⁹¹ However, even by small changes of the composition, it is possible to modify the surface mechanical properties.^{91–96}

1.3 | The LIMEs project

The LIMEs project (Light Innovative Materials for Enhanced Solar Efficiency) was a Solar-ERA.NET project that ran from 2014 to 2017, which investigated cover glass properties for PV applications. Solar-ERA.NET was an EU FP7 funded network that since 2013 has launched joint calls to strengthen the competitiveness and innovativeness of European industry. In these calls, one of the key topics has been 'Solar glasses and encapsulation materials'. The LIMEs project addressed several aspects that are relevant for PV cover glasses and investigated optical,⁶³ mechanical and chemical properties of glass as well as novel thermal toughening methods⁹⁷ and also the addition of antireflective and self-cleaning capabilities to the glass surface.^{98,99} The glasses made in laboratory experiments were used for proof-of-concept studies by making the 70 × 70 mm PV modules discussed here. These aspects were addressed in order to give the opportunity to make thinner cover glasses that give enhanced efficiency and increased lifetime of PV modules. This paper gives an overview of some of the results and knowledge gained from this project and since.

2 | EXPERIMENTAL PROCEDURES

2.1 | Glass synthesis

In the LIMEs project, several different glass synthesis routes were used in order to optimize given properties within each subset of glasses. These are described below.

TABLE 1 Design of experiments variation of compositions given in mol%

Oxide	1st DoE	2nd DoE
SiO ₂	71.36 to 66.36	70.76
Al ₂ O ₃	0 to 5	0.59
B ₂ O ₃	0 to 5	0
Na ₂ O	13.93	13.93
CaO	9.24	5 to 14.71
MgO	5.47	0 to 8.
TiO ₂	-	0 to 5
BaO	-	0 to 5
ZnO	-	0 to 5
ZrO ₂	-	0 to 5
SrO	-	0 to 2.5
La ₂ O	-	0 to 2

2.1.1 | Glass synthesis for optimizing mechanical and chemical properties

Glass was produced using high-purity ($\geq 99.9\%$ purity) raw materials from Glasma AB (MAM1s Sand, $\text{Al}(\text{OH})_3$, $\text{Na}_2\text{B}_4\text{O}_7 \cdot 5\text{H}_2\text{O}$, Na_2CO_3 , $\text{CaMg}(\text{CO}_3)_2$, CaCO_3 , MgO , SrCO_3 , BaCO_3 , Na_2SO_4 , TiO_2 , ZnO , ZrO_2 and La_2O_3). Glass melting was performed in Pt/Rh crucibles using an electrically heated Super Kanthal furnace at 1450°C for 2 h, homogenization by stirring at 1400°C for 1 h, conditioning for 1.5 h at 1450°C and finally 0.5 h at 1480°C to improve pourability. The glass was poured into stainless steel moulds with rectangular shape (ca. $50 \times 40 \times 10$ mm) and was annealed from 540°C for 1 h and then cooled to ambient temperature. The software MODDE from UMETRICS was used for the design of experiments (DoEs). In the first DoE, 12 glasses evaluate the network formers SiO_2 , B_2O_3 and Al_2O_3 , whereas MgO , CaO and Al_2O_3 were kept constant; see Table 1. In the second DoE, the network modifiers were evaluated in 15 glass melts. The relative component influence on the different evaluated properties described in Sections 2.2 and 2.3 was then evaluated based on the authors' collective glass technological expertise.

2.1.2 | Glass synthesis for optimizing optical properties

Raw materials were high purity (<100 ppm Fe) silica sand, and $\geq 99.9\%$ purity aluminium hydroxide ($\text{Al}(\text{OH})_3$), sodium carbonate (Na_2CO_3), calcium carbonate (CaCO_3), magnesium carbonate (MgCO_3), bismuth oxide (Bi_2O_3) and sodium sulphate (Na_2SO_4). All raw materials were dried at 110°C for 24 h prior to batch preparation. Batches to produce 100 g of glass of the compositions shown in Table 2 were prepared using a three-decimal place balance, mixed thoroughly and then melted in a zirconia grain stabilized platinum (ZGS-Pt) crucible in an electric furnace for 5 h at 1450°C . Homogenous, bubble-free glasses were then poured into steel moulds, cooled until sufficiently stiff to

remove the moulds without distortion, and then placed in a second electric furnace and annealed for 1 h at 530°C to remove thermal stresses, before cooling within the furnace to room temperature over 6 h. Samples for optical absorption measurements were ground with SiC paper with progressively smaller particle sizes to $1 \mu\text{m}$, then polished using a $1 \mu\text{m}$ CeO_2 polishing slurry.

2.1.3 | Flat glass synthesis for solar cells and solar cell efficiency measurements

Raw materials were high purity (100 ppm Fe) silica sand, and $\geq 99.9\%$ purity aluminium hydroxide ($\text{Al}(\text{OH})_3$), sodium carbonate (Na_2CO_3), calcium carbonate (CaCO_3), magnesium carbonate (MgCO_3), bismuth oxide (Bi_2O_3), gadolinium oxide (Gd_2O_3) and sodium sulphate (Na_2SO_4). All raw materials were dried at 110°C for 24 h prior to batch preparation. Batches to produce 100 g of glass of the compositions shown in Table 3 were prepared using a three-decimal place balance, mixed thoroughly and then melted in a zirconia grain stabilized platinum (ZGS-Pt) crucible in an electric furnace for 5 h at 1450°C . Glasses were then poured into a steel mould that was preheated to 550°C , as illustrated in Figure 5. The inclusion of nearly 2-mol% Li_2O in each glass composition was found to be necessary to reduce the viscosity sufficiently to enable reproducible forming of the 7×7 cm plates that were needed for solar performance testing. Although this compositional change represents a slight departure from current float glass compositions,¹⁰⁰ manufacture of similar glass compositions has been successfully trialled and demonstrated at commercial scale¹⁰⁰ supporting the applicability of the glass compositions studied here. Here, during forming, excess glass passed through the overflow channels. Once the plates were formed, the mould was removed, and the glass was subsequently annealed at 530°C for 1 h before cooling slowly to room temperature. Samples for optical absorption measurements were ground with SiC paper with progressively smaller particle sizes to $1 \mu\text{m}$ and then polished using a $1\text{-}\mu\text{m}$ CeO_2 polishing slurry. A

TABLE 2 Glass compositions (mol%) and measured densities

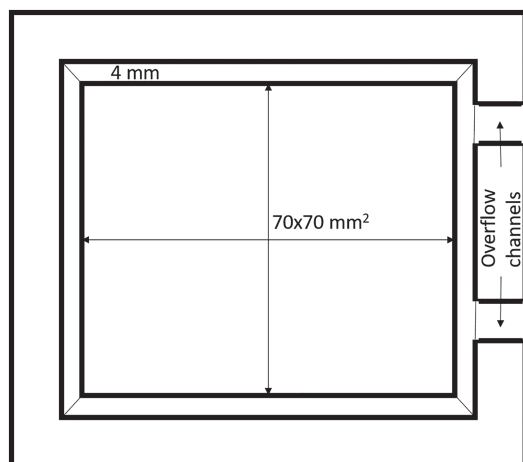
Sample name	SiO_2	Al_2O_3	MgO	CaO	Na_2O	SO_3	Bi_2O_3	Fe_2O_3	Density ($\text{g}/\text{cm}^3 \pm 0.002$)
Base glass	70.51	0.59	5.48	9.25	13.95	0.22	0.00	0.00	2.484
Base glass*	72.00	0.48	5.01	9.13	13.20	0.18	<0.10	<0.10	
0.01	70.50	0.59	5.48	9.25	13.95	0.22	0.01	0.00	2.485
0.025	70.485	0.59	5.48	9.25	13.95	0.22	0.025	0.00	2.487
0.05	70.46	0.59	5.48	9.25	13.95	0.22	0.05	0.00	2.497
0.10	70.41	0.59	5.48	9.25	13.95	0.22	0.10	0.00	2.502
0.15	70.36	0.59	5.48	9.25	13.95	0.22	0.15	0.00	2.513
0.20	70.31	0.59	5.48	9.25	13.95	0.22	0.20	0.00	2.518
0.20/0.01	70.30	0.59	5.48	9.25	13.95	0.22	0.20	0.01	2.518
0.20/0.05	70.26	0.59	5.48	9.25	13.95	0.22	0.20	0.05	2.519
0.20/0.10	70.21	0.59	5.48	9.25	13.95	0.22	0.20	0.10	2.523

Note. All are nominal compositions except where noted, as analysed by XRF.

*Analysed by XRF.

TABLE 3 Nominal compositions (mol%) of soda–lime–silica flat glass samples for PV testing

Sample name	SiO ₂	Al ₂ O ₃	MgO	CaO	Na ₂ O	Li ₂ O	Na ₂ SO ₄	Bi ₂ O ₃	Gd ₂ O ₃
LIMES base glass	69.29	0.58	5.38	9.09	13.48	1.96	0.22	0.00	0.00
LIMES B2	69.09	0.58	5.38	9.09	13.48	1.96	0.22	0.20	0.00
LIMES BG A, B, C	69.09	0.58	5.38	9.09	13.48	1.96	0.22	0.10	0.10
LIMES B2G2	68.89	0.58	5.38	9.09	13.48	1.96	0.22	0.20	0.20
LIMES B2G A, B	69.99	0.58	5.38	9.09	13.48	1.96	0.22	0.20	0.10

**FIGURE 5** Plan view schematic of the steel mould used to prepare 7 × 7 cm flat glass samples

base glass (LIMES A) similar to float glass (with the aforementioned Li₂O additions to enable forming) was prepared, and seven further glasses containing different levels of Bi₂O₃ and Gd₂O₃ (see Allsopp et al.⁶⁴) were prepared, as shown in Table 3.

2.2 | Glass characterization

2.2.1 | Mechanical property, density and compositional analyses

Densities were measured on solid bulk glass samples (with mass 10–30 g) using the Archimedes method and a four-decimal place balance with deionized water at 20°C. The measured densities presented in Table 2 are averages of three independent measurements. Densities, presented in Table 2, are consistent with other experimental values⁹⁵ and the Fluegel model,¹⁰¹ indicating the compositions is similar to the nominal compositions, also shown in Table 2.

Mechanical properties were investigated using nanoindentation/microindentation. The employed instrument was an Anton Paar Micro Combi tester equipped with a CPX-NHT² nanoindenter. Vickers indenter tip was used for the microindentation measurements and for the nanoindentation a Berkovich tip. Average hardness and reduced elastic modulus from 20 indents were measured using the nanoindentation. Indentation fracture toughness and

crack resistance (CR) were measured using microindentation by collecting 10 and 15 indents, respectively. We followed the conventional scheme of indentation fracture toughness¹⁰² and CR.^{103,104}

X-ray fluorescence (XRF) analyses were carried out using a Phillips Magix Pro XRF spectrometer and a Panalytical Axios Fast fluorescence spectrometer using a 1:10 sample to lithium tetraborate flux ratio as fused beads. Beads were melted in a Pt/5%Au crucible at 1065°C for 15 min then cooled in the air to room temperature. Scans were carried out on the SuperQ 3-IQ + software in the oxide setting. XRF analysis of the base glass, shown in Table 2, corresponds to the expected values from the nominal composition.

2.2.2 | Chemical resistance and weathering analysis

The chemical resistance was determined by the powder method, standardized as ISO 719, commonly called P₉₈. It is a hydrolytic method involving cooking of 1-g glass powder with fractions in the range of 100–300 µm for 1 h at 98°C. The water is then titrated with 0.01 N HCl and the result expressed as consumed ml of 0.01 N HCl per g of glass.

Climate chamber tests were conducted in a climate box to verify the P₉₈ results. The method employed involved subjecting the samples to 50°C with approximately 100% relative humidity for 3 weeks. UV-Vis spectrophotometry was used for evaluating the results. The glass samples (ca. 40 × 20 × 10 mm) were mounted in the metal holder for grading and polishing. The smaller side was polished with three different grades of diamond grading wheels (125, 320 and 600 µm) for 2 min each. Final polishing used a diamond paste (1 µm) for 6 min. In order to calculate the visible light transmittance of the glass T_v , Equation 1) was adopted from EN 410:2011. The term $D_\lambda V(\lambda)$ $D_\lambda \cdot 10^2$ is given in tabular form in the EN 410:2011.

$$\tau_v = \frac{\sum_{\lambda=380\text{nm}}^{\lambda=780\text{nm}} D_\lambda \tau(\lambda) V(\lambda) \Delta\lambda}{\sum_{\lambda=380\text{nm}}^{\lambda=780\text{nm}} D_\lambda V(\lambda) \Delta\lambda} \quad (1)$$

The transmission was measured between 380 and 780 nm with a PerkinElmer UV-VIS spectrophotometer (Lambda 25) using a scan speed of 480 nm/min, collecting interval 10 nm and a slit width of 1 nm. The light source switch between UV-VIS occurs at 326 nm. The transmission was measured before and after treatment in a climate chamber.

2.2.3 | Thermal property analyses

Thermal expansion behaviour was determined using a dilatometer from room temperature to the softening temperature with a speed of 25 K/min. The determined parameters are thermal expansion (α), transformation temperature T_g and softening temperature, M_g . A glass rod of 40- to 50-mm length and a diameter of 5 mm was used.

For determining the liquidus temperature, the glass was crushed and sieved to the fractions 1–3 mm and placed on a platinum ship. The liquidus temperature was determined in a gradient furnace in the temperature interval of 930–1200°C for 8 h. The resulting amount of crystals was controlled in a polarized light microscope.

Theoretical calculations of the high-temperature viscosity of given glass compositions were performed using the Lakatos factors for the SLS system for the base glass and the crystal glass system for the others.¹⁰⁵ The results are displayed as the parameters of the Vogel–Fulcher–Tammann equation, $T = T_o + B/(\log \eta + A)$ and as $(\log (\eta/\text{dPas}))$ versus temperature (°C).

2.2.4 | Optical property analyses

Optical absorption UV–Vis–NIR spectra were measured between 200 and 1100 nm using a Varian Cary 50 spectrophotometer, at a rate of 60 nm/min and with a data interval of 0.5 nm. UV–Vis–NIR fluorescence measurements were carried out using a Varian Cary Eclipse spectrophotometer with all samples placed at 30° to normal incidence. Excitation and emission measurements were made using a 120-nm/min scan rate and 1-nm data interval with slit widths of 20 or 10 nm, and a detector voltage of 400 V.

2.3 | Solar cell manufacturing and solar cell efficiency characterization

Solar modules exemplified by that shown in Figure 6 were prepared at Solar Capture Technologies Ltd, Blyth, UK. Wafers of c-Si (ALBSF Monocrystalline 20.2% efficiency, size 20 × 11 mm, eight cells in series) were tabbed using an Ag PV tabbing ribbon (width 1.2 mm), Tedlar backsheet (Feron CPx 1000), EVA glue (EVASA Solarcap FC100011E 0.46-mm thickness) and glass front sheet (as described in Section 2.1.3). These were cured to form test modules such as that shown in Figure 6. The exact details of the temperature, time and pressure for lamination of the PV modules are the propriety technology of Solar Capture Technologies and are not available within this manuscript. To enable comparison of the candidate glasses against a benchmark, commercially available float glass was obtained and prepared into a module in the same way as the candidate glasses. Electroluminescence measurements were carried out to identify damaged areas. Solar efficiency measurements were performed on each test module using solar simulator device, SPI-SUN SIMULATOR 240A, with 1.5 AM illumination (Global terrestrial conditions), as described in

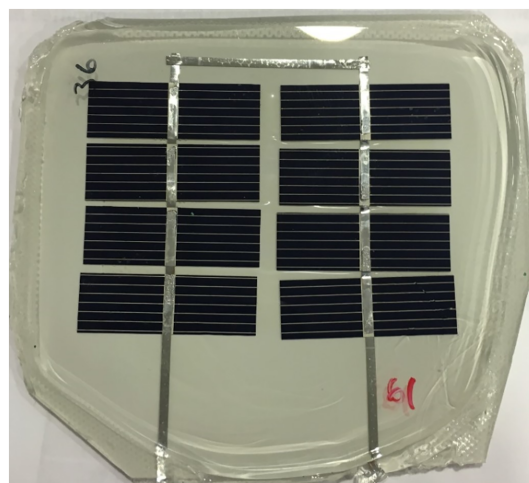


FIGURE 6 Representative PV module prepared at Solar Capture Technologies Ltd, Blyth, UK [Colour figure can be viewed at wileyonlinelibrary.com]

previous studies.¹⁰⁶ The solar simulator was using a pulsed Xenon light source that closely matches the solar spectrum that with filtering meets ASTM E-927 spectral distributions. The SUN SIMULATOR provides in addition to an *I*–*V* curve display, a parametric evaluation of the solar module, which include open-circuit voltage (V_{OC}), short-circuit current (I_{SC}), peak power at load (P_{VLD}), peak voltage at load (V_{LD}), peak current at load (I_{VLD}), cell or module efficiency (EF), fill factor (FF), peak power (P_{MAX}), voltage at peak power (V_{MAX}), current at peak power (I_{MAX}), shunt resistance (R_{SH}), series resistance (R_S). The results were corrected to standard testing conditions (1000 W and 25°C). The perimeter of the module was masked and placed in the same location in the centre of the solar simulator that was calibrated before use. Both strings (unlaminated with EVA and cover glass) and modules (laminated with EVA and cover glass) were measured to enable comparison of differences arising during processing.

3 | RESULTS AND DISCUSSION

3.1 | Glass results

3.1.1 | Optimization of glass compositions for use as cover glass for PV modules

Two different glass series have been manufactured, based on modifying the base glass composition that is similar to conventional float glass compositions (see Table 4), thus remaining technologically relevant while enabling exploration of potentially achievable compositional modifications (see, e.g., Wallenberger and Bingham¹⁰⁰). In total 27 different glasses were developed through a DoEs program to evaluate the varied components effect on the properties; see Table 1 and Section 2.1.1 for details. The DoEs resulted in information on the relative influences of each component on the different properties. The DoE information was then used for proposing three different

TABLE 4 Glass compositions (mol%) resulting from the design of experiments (DoEs) of 27 glasses, compare Table 1

Sample name	SiO ₂	Al ₂ O ₃	Na ₂ O	CaO	MgO	ZnO	TiO ₂	SO ₃
Base glass	70.6	0.6	13.9	9.2	5.5	-	-	0.2
LIMES A	70.7	2.0	13.9	3.15	6.0	2.0	2.0	0.2
LIMES B	70.9	2.0	13.9	5.0	3.15	5.0	-	0.2
LIMES C	70.9	1.0	13.9	5.0	3.15	5.0	1.0	0.2

Note: A conventional float glass composition was used as base glass composition.

TABLE 5 Mechanical and chemical property characterization results

Sample name	Hardness (GPa)	Reduced elastic modulus (GPa)	Crack resistance (N) ¹⁰³	P ₉₈ (ISO 719)	Climate chamber treatment in ΔT%
Commercial float glass	6.9 ± 0.1	73.7 ± 0.4	0.5 ± 0.1	1.20 ± 0.1	-
Base glass	7.3 ± 0.1	73.3 ± 0.7	1.0 ± 0.1	0.85 ± 0.1	-2.5 ± 0.5
Glass A	7.1 ± 0.1	71.9 ± 0.4	1.3 ± 0.1	0.47 ± 0.1	0.23 ± 0.5
Glass B	7.3 ± 0.1	72.4 ± 0.6	1.5 ± 0.1	0.43 ± 0.1	0.04 ± 0.5
Glass C	7.3 ± 0.1	73.4 ± 0.3	0.6 ± 0.1	0.46 ± 0.1	-1.76 ± 0.5

Note: P₉₈ is given with the unit ml 0.01 N HCl per gramme glass.

compositions (A, B and C), which were then evaluated separately. The decision was made by a trade-off between glass processing and the improvement in properties based partly on the DoE and partly on our collected glass technological know-how. The proposed glass compositions (A, B and C) mechanical properties were investigated using nanoindentation/microindentation (results are shown in Table 5). Hardness and elastic modulus (stiffness) were found to be relatively constant, whereas the parameter CR¹⁰³ was significantly increased for the optimized compositions, most notably compositions A and B that were approximately increased with a factor of 3.

Chemical properties were studied through combined climate testing and UV-Vis spectroscopy as well as P₉₈ (ISO 719). Both climate testing and P₉₈ show comparable trends in the results. The methods both represent ageing of the glass and the climate test more akin to weathering,¹⁰⁷ whereas the P₉₈ evaluates the hydrolytic resistance of glass compositions. In Table 5, the climate chamber tests (expressed as ΔT%, before and after climate testing) and the P₉₈ results are shown. The optimized glasses (A, B and C) give approximately a factor of two performance improvement compared with conventional float glass. In order to simulate 30 years of environmental exposure, an

empirical equation developed by Lyle¹⁰⁸ was used to calculate the parameters of the climate chamber tests. The optimized glasses being tested for 30 years of usage show longer service lifetime than float glass (approximately a factor of 2). Alumina is known to have a positive effect on the chemical resistance.^{109,110} Besides that, based on previous literature are Sn, Ag, Bi, Ti, Ba, Sr, La, Zn, Mg and Zr interesting oxides for the improvement of the chemical durability.¹¹¹⁻¹¹³ Based on the results in Table 5, glass B shows the most promising results.

Optimization of the mechanical and chemical properties is of course interesting and important from a PV perspective; however, the thermal properties remain the most important from the perspective of being able to manufacture the glass. In order to estimate the feasibility of glass production, a number of basic thermal properties were measured (see Table 6) and the viscosity calculated (see Table 7). The thermal expansion coefficients of glasses A, B and C were measured as it is an important property for the thermal strengthening of glass, the lower the thermal expansion coefficient is, the lower the strengthening degree will become for a given quench rate.¹¹⁴ The thermal

TABLE 6 Results for the thermal property characterization

Sample name	α_{25-300° (10 ⁻⁶ K ⁻¹)	T _g (°C)	M _g (°C)	T _{Liq} (°C)
Base glass	8.90 ± 0.1	554 ± 5	615 ± 5	1120 ± 20
Glass A	7.02 ± 0.1	569 ± 5	630 ± 5	1080 ± 20
Glass B	8.27 ± 0.1	554 ± 5	605 ± 5	No crystals
Glass C	8.26 ± 0.1	554 ± 5	614 ± 5	1108 ± 20

Note: α_{25-300° is the thermal expansion coefficient; T_g, the dilatometric glass transition temperature; M_g, the dilatometric softening temperature and T_{Liq}, the liquidus temperature.

TABLE 7 Results for the theoretical calculations of the viscosity curves using Lakatos factors displayed as log viscosity data (2, 3 and 5) as well as Vogel-Fulcher-Tammann parameters (A, B and T₀)¹⁰⁵

Sample name	Log $\eta = 2$ (dPas)	Log $\eta = 3$ (dPas)	Log $\eta = 5$ (dPas)	A	B	T ₀
Base glass	1435°C	1181°C	902°C	1.65	4312.81	252.90
Glass A	1466°C	1180°C	901°C	0.83	3106.66	367.94
Glass B	1469°C	1193°C	903°C	1.35	4018.10	269.80
Glass C	1439°C	1174°C	892°C	1.36	3896.73	279.73

expansion coefficients are slightly lowered compared with the base glass but still sufficiently high for thermally strengthen the glass.⁷⁴ The results of the glass transition temperature (T_g), liquidus temperature (T_{liq}) and viscosity are similar to the base glass composition. Measured thermal expansion coefficients of glasses A, B and C are similar to conventional float glass, which is sufficient for the possibility to thermally strengthen these compositions.

3.1.2 | Doping of optically active components for UV down-shifting

As shown in Figure 7, compare Table 2, the UV-Vis-nIR absorption spectra of SLS glasses doped with 0- to 0.2-mol% Bi_2O_3 all show a strong UV absorption edge, even in the Bi_2O_3 -free glass. This UV absorption in the Bi_2O_3 -free glass is due to the Si-O network and network modifying cations, with contributions from parts-per-million levels of Fe^{2+} and Fe^{3+} occurring as impurities from the raw materials used to make the glasses. The incorporation of Bi in the glasses has the effect of shifting the UV absorption to lower wavenumbers (longer wavelengths). This is attributable to $^1\text{S}_0 \rightarrow ^3\text{P}_0$ and $^1\text{S}_0 \rightarrow ^3\text{P}_1$ transitions of Bi^{3+} , causing strong, broad absorption bands centred in the deep UV with tails to lower wavenumbers. Similar behaviour was recently observed for $s \rightarrow p$ transitions of Sb^{3+} -doped float-type SLS glasses⁶⁵; however, the nontoxicity of Bi renders it preferable to Sb from a health and safety perspective. Increasing Bi concentrations thus increase the intensity of these UV absorption bands and hence shift the UV edge to lower wavenumbers (longer wavelengths). The addition of only 0.01-mol% Bi_2O_3 shifts the UV edge by 1200 cm^{-1} (11 nm) compared with the Bi-free (base) glass. The dotted line shown in Figure 7 is reproduced from Yang et al¹¹⁵ and extended using data from Fix et al¹¹⁶ and provides the absorption profile of C-EVA. This

can change, depending on composition and age of the C-EVA¹¹⁷ or T-EVA (see Section 1) and older; more strongly irradiated EVA will exhibit a shift in its absorption profile to lower wavenumbers (longer wavelengths).

The effects on optical absorption spectra of doping SLS glasses with different levels and combinations of Bi_2O_3 and Fe_2O_3 are shown in Figure 8, with compositions given in Table 2. Increasing levels of Fe_2O_3 shift the UV edge to lower wavenumbers (longer wavelengths) as expected. The narrow absorption band at $26\,220\text{ cm}^{-1}$ (381 nm) is attributed to the $^6\text{A}_1(\text{S}) \rightarrow ^4\text{E}(\text{D})$ transition of Fe^{3+} cations in tetrahedral and octahedral sites within the glass structure.^{34,58-60} The broad absorption band centred at $10\,000\text{ cm}^{-1}$ (1000 nm) is attributed to the $^5\text{T}_2(\text{D}) \rightarrow ^5\text{E}(\text{D})$ transition for Fe^{2+} ions in octahedral sites, which decreases transmission of photons close to the bandgap of c-Si solar cells (1.14 eV or 1087 nm), thereby deleteriously affecting solar cell efficiency.

Fluorescence excitation and emission spectra are shown in Figure 9. The emission spectrum arises from excitation at $33\,300\text{ cm}^{-1}$ (300 nm). It can be observed that emission intensity increases with increasing Bi_2O_3 concentration throughout the series studied, and consequently, we can conclude that concentration quenching did not strongly impact upon emission intensity within the range of Bi_2O_3 additions studied here. The emission band is broad (half-width half-maximum is estimated to be approximately 2500 cm^{-1}) and centred at $23\,700\text{ cm}^{-1}$ (430 nm), with a second, weak band centred at $12\,800\text{ cm}^{-1}$ (780 nm). The two excitation spectra (shown as dotted lines in Figure 9) illustrate that the two emission bands have different origins and are centred at approximately $33\,000\text{ cm}^{-1}$ (300 nm) and $30\,500\text{ cm}^{-1}$ (328 nm), respectively.

Fluorescence emission spectra (Figure 10) show the emission, as a function of excitation wavenumber, for Sample 0.20, as given in Table 2. Within the deep UV, there are inefficiencies of absorption because of the photons having higher energy than the bandgap of

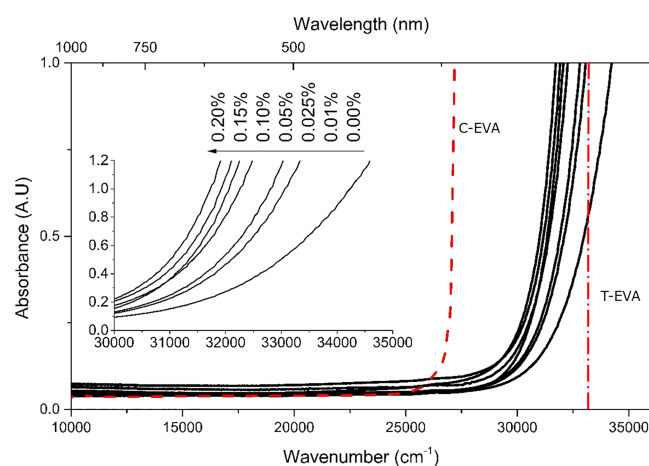


FIGURE 7 UV-Vis-nIR absorption spectra of Bi_2O_3 -doped soda-lime-silica glasses (compositions given in Table 2). The red dotted line corresponds to the absorption profile of C-EVA glue and the approximate T-EVA UV cut-off. The inset figure shows the effect on UV edge position of increasing Bi_2O_3 content (mol%) [Colour figure can be viewed at wileyonlinelibrary.com]

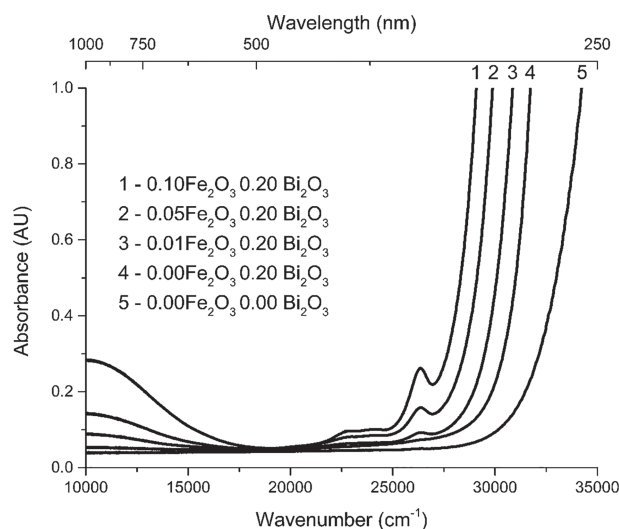


FIGURE 8 UV-Vis-nIR absorption spectra of $\text{Fe}_2\text{O}_3 + \text{Bi}_2\text{O}_3$ -doped (mol%) soda-lime-silica glasses (compositions given in Table 2)

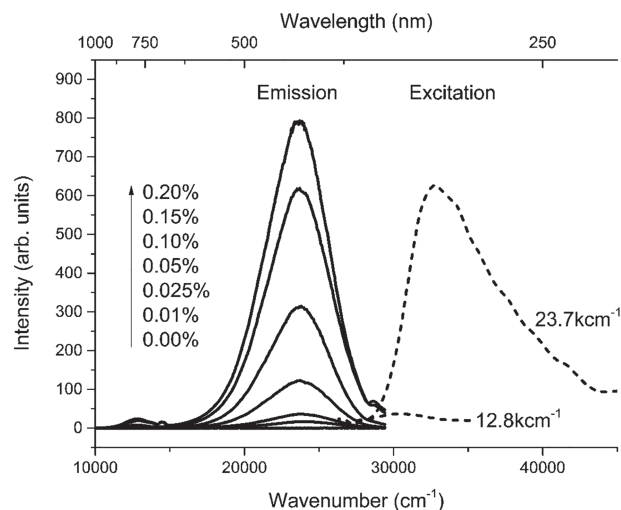


FIGURE 9 UV-Vis-nIR fluorescence excitation (dotted) and emission (solid) spectra for Bi_2O_3 -doped soda-lime-silica glasses (mol%). Nominal compositions are given in Table 2

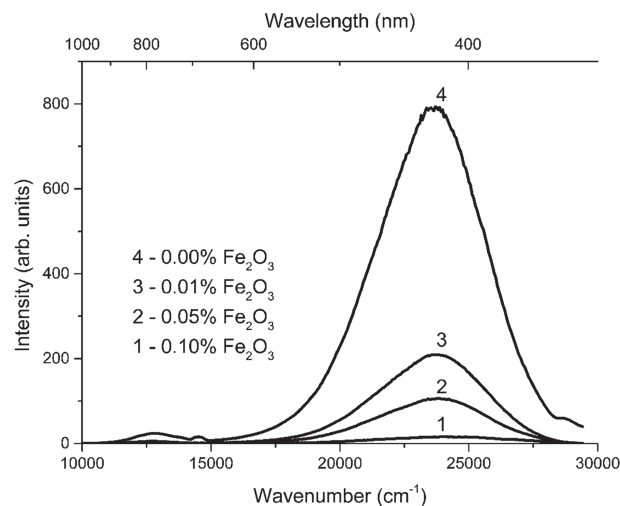


FIGURE 11 FUV-Vis-nIR fluorescence emission spectra of 0.20-mol% Bi_2O_3 -doped soda-lime-silica glass ($33\,300\text{ cm}^{-1}/300\text{-nm}$ excitation) as a function of increasing Fe_2O_3 content (mol%). Nominal compositions given in Table 2

Bi^{3+} , between $35\,700\text{ cm}^{-1}$ (280 nm) and $33\,300\text{ cm}^{-1}$ (300 nm) shows the greatest emission intensity.

Figure 11 shows the effects on fluorescence emission spectra from the 0.20-mol% Bi_2O_3 -doped SLS glass (Sample 0.2 from Table 2) as a function of increasing added Fe_2O_3 (mol%). Through a combination of competitive absorption of UV photons and fluorescence quenching, the total intensity of the Bi^{3+} emissions decreases strongly with increasing Fe_2O_3 concentration, illustrating the need to minimize Fe_2O_3 content to enable maximum visible fluorescence from Bi^{3+} .

Optical measurements were carried out on flat and polished glass samples with thickness $8 \pm 0.1\text{ mm}$. The UV absorption edge in glasses is characterized by a cut-off wavelength corresponding to photon energies high enough to induce absorption.¹¹⁸ To enable comparative study, we have set this here to the wavenumber corresponding to absorption of 1.0. From Figure 8, we show that increasing additions of Fe_2O_3 to the glass cause a shift in the UV edge towards the visible region. The addition of only 0.01-mol% (100 ppm) Fe_2O_3 to silicate

glass as a PV module cover glass has been shown to reduce the module output by 1.1% because of the visible and IR absorptions at $26\,220$ and $11\,000\text{ cm}^{-1}$ (381 and 909 nm) of Fe^{3+} and Fe^{2+} , respectively.³⁵ By comparison, the addition of Bi_2O_3 to these glasses can provide a degree of UV protection to the C-EVA and the T-EVA glue, as shown in Figure 7, but without any of the deleterious visible or nIR absorption bands, shown in Figure 8, that arise from doping the solar glass with Fe_2O_3 .

C-EVA strongly absorbs photons with wavenumbers above $26\,666\text{ cm}^{-1}$ (wavelengths below 375 nm),¹¹⁵ with damage arising from absorption of photons with higher energies than this. Similarly, and as discussed in Section 1, T-EVA also suffers, albeit to a lesser extent than C-EVA, from damage due to high-energy photons. For C-EVA, which remains widely used in the PV industry, the National Renewable Energy Laboratory (NREL) carried out a study of the yellowing index of EVA glues in Si-based PV modules.¹¹⁹ In their

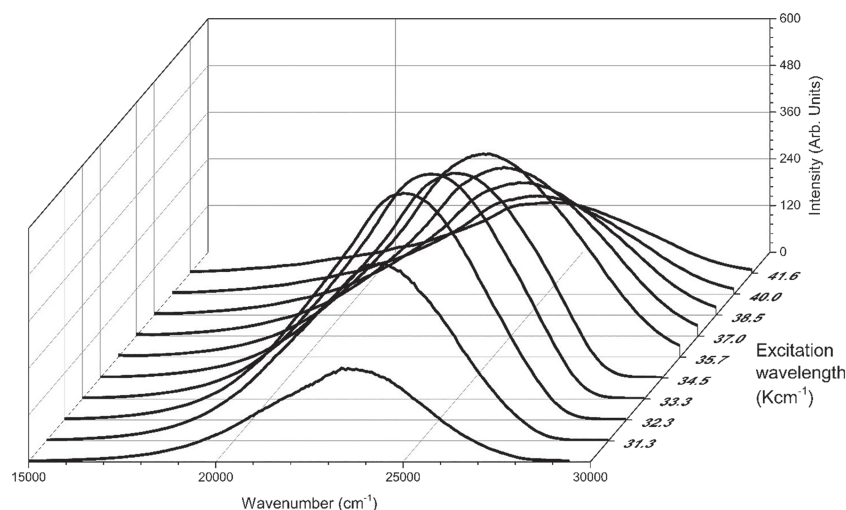
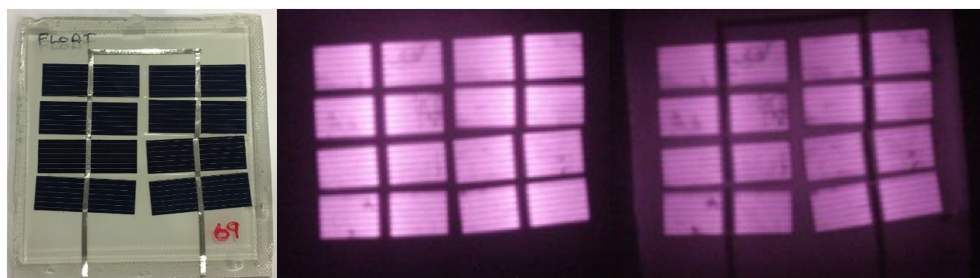


FIGURE 10 UV-Vis-nIR fluorescence emission spectra of 0.20-mol% Bi_2O_3 -doped soda-lime-silica glass as a function of excitation wavenumber

FIGURE 12 Float glass PV module (left) and electroluminescence of string (centre) and module (right) float glass PV module [Colour figure can be viewed at wileyonlinelibrary.com]



study, the module was covered with a standard SLS glass, with UV edge at $33\,900\text{ cm}^{-1}$ (295 nm). They observed that the yellowing index was 81.9 after 35 weeks of accelerated ageing. They also studied PV modules covered with two SLS glasses, doped with 0.3- and 1.0-mol% CeO_2 respectively, which had been added to the glass to move the UV edge to lower wavenumbers of $30\,770\text{ cm}^{-1}$ (325 nm) and $30\,300\text{ cm}^{-1}$ (330 nm). The two glasses presented yellowing indices of 23.8 (0.3-mol % CeO_2) and 17.8 (1.0-mol% CeO_2), under the same accelerated ageing conditions. It is believed that the Bi_2O_3 -doped glasses studied here may be suitable to achieve similar or greater levels of UV solar protection, given appropriate optimization. These glasses also require lower concentrations of Bi_2O_3 than the CeO_2 glasses. Control of the UV absorption edge to even more effectively match the C-EVA absorption 'edge' would require considerably higher doping concentrations than those that we have studied here and may produce undesirable visible absorption bands centred at $20\,000\text{ cm}^{-1}$ (500 nm) and $14\,300\text{ cm}^{-1}$ (700 nm), as shown for other glasses doped with 1.0-mol% Bi_2O_3 .¹²⁰ However, T-EVA now represents a number of apparent improvements over C-EVA in terms of its UV transparency. Consequently, lower levels of cover glass dopants such as Bi^{3+} than are necessary to fully protect C-EVA may be sufficient to provide protection of T-EVA components of PV modules, which could in turn render the economic considerations for using such glasses even more favourable.

As demonstrated in Figure 10, there is a large variation in emission intensity as a function of excitation wavelength. The peak is consistently centred at $23\,700\text{ cm}^{-1}$ (420 nm) with little variation. Although at sea level there are few photons with high energies in the deep UV ($>33\,000\text{ cm}^{-1}$, $<300\text{ nm}$), there is strong absorbance of these highly damaging photons as shown in Figure 7 because of the transition of $^1\text{S}_0 \rightarrow ^3\text{P}_1$.⁶² Bi^{3+} ion has a $6s^2$ electronic configuration and has the ground state $^1\text{S}_0$. After an electron has been promoted to a vibrational level in the $^3\text{P}_1$ state, the electron will relax to the lower $^3\text{P}_0$ through a nonradiative transition at lower temperatures (4.2 K), and the forbidden $^3\text{P}_0 \rightarrow ^1\text{S}_0$ emission state is predominantly observed.¹²¹ However, at room temperature, the electron in the $^3\text{P}_1$ state directly radiates to the $^1\text{S}_0$ state and is the preponderant emission.¹²² Xu et al demonstrated that concentration quenching of Bi^{3+} ions in borate glasses occurs above 0.25-mol% Bi_2O_3 and leads both to a reduction in emission intensity and to a shift to longer wavelengths of the peaks.⁶² This has been attributed to the self-absorption of Bi^{3+} , that is, photons emitted through UV-induced fluorescence are significantly more likely to be reabsorbed because of the higher quantity of Bi^{3+} centres.⁶² Within this study,

the doping concentration of Bi_2O_3 has been maintained below 0.20 mol% to both prevent deleterious visible absorptions and to minimize self-absorption effects.

Figure 11 displays the effect of increasing Fe_2O_3 concentration on the fluorescence emission of Bi^{3+} excited at $33\,300\text{ cm}^{-1}$ (300 nm). The total emission rapidly diminishes with increasing quantities of Fe_2O_3 . As shown in Figure 8, the UV absorption of $\text{Fe}_2\text{O}_3/\text{Bi}_2\text{O}_3$ -doped is shifted further towards the visible than the corresponding Bi_2O_3 and base glass. This is attributed to the $^6\text{A}_1(\text{S}) \rightarrow ^4\text{T}_2(\text{D})$ transition of Fe^{3+} with a peak position at $25\,190\text{ cm}^{-1}$ (396 nm) and the $^6\text{A}_1(\text{S}) \rightarrow ^4\text{E}(\text{D})$ with a peak position at $27\,250\text{ cm}^{-1}$ (366 nm).³⁴ Although Fe_2O_3 more strongly shifts the UV edge and therefore better protects the EVA from damage, the visible and IR bands deleteriously impact PV module efficiency, up to 9.8% loss with a 0.10-mol% Fe_2O_3 -doped glass front sheet.³⁵ The authors postulate small doping concentrations (up to 0.20 mol%) of Bi_2O_3 may protect the EVA from UV-induced degradation without the visible and IR bands associated with Fe_2O_3 .

3.1.3 | Thermal strengthening of glass and in situ chemical vapor deposition

In a previous publication,⁹⁷ we have demonstrated the combination of thermal strengthening of glass and the application of amorphous Al_2O_3 coating onto the glass. This was demonstrated using MOCVD and Al (ac-ac)₃ as the precursor with the purpose to increase the surface mechanical properties and tentatively also the chemical durability. The latter has however not been studied. The elaborated process produced thermally strengthened glass of similar strengthening level as conventional tempered glass, that is, 80–110 MPa.¹²³ The Al_2O_3 content was quantified being at least doubled at the surface and having an increased Al_2O_3 content at least $0.5\text{ }\mu\text{m}$ into the glass surface. The surface mechanical properties were characterized using the CR method,¹⁰³ showing a value of 1.3 N compared with 0.8 N for traditional thermal strengthening.

3.2 | Solar cell efficiencies as a function of glass composition

A float glass PV module is shown in Figure 12 (left), the electroluminescence of before defined as string (centre) and after lamination defined as module (right), and a typical I/V curve is shown in

TABLE 8 Electrical data of PV modules

		Float	LIMES A	LIMES BG A	LIMES BG B	LIMES BG C	LIMES B2G A	LIMES B2G B	LIMES B2G2	LIMES B2
Property	Uncertainty	Modules								
Irradiance (W/m ²):	±20	1044	1041	1062	1057	1040	1040	1051	1043	1051
Corrected (W/m ²):	±20	1000	1000	1000	1000	1000	1000	1000	1000	1000
Module temp (°C)	±1	23.4	24.0	24.0	23.8	21.8	22.2	23.1	23.2	22.9
Corrected to (°C)	±1	25	25	25	25	25	25	25	25	25
V _{OC} (V)	±0.3	5.07	4.97	4.98	5.01	4.99	4.97	5.05	5.03	4.97
I _{SC} (A)	±0.003	0.113	0.062	0.070	0.113	0.115	0.114	0.117	0.111	0.115
R _{series} (mΩ)	±10	45.20	7.06	85.16	11.18	6.18	15.51	14.37	18.50	5.59
R _{shunt} (Ω/cm ²)	±100	626.67	6460.12	4206.23	986.97	4838.96	504.53	1004.53	576.77	983.19
P _{max} (W)	±0.02	0.445	0.241	0.284	0.434	0.467	0.429	0.465	0.437	0.446
V _{pm} (V)	±0.4	4.33	4.66	4.35	4.17	4.28	4.13	4.27	4.25	4.15
I _{pm} (A)	±0.005	0.103	0.052	0.065	0.104	0.109	0.104	0.109	0.103	0.107
Fill factor	±0.05	0.78	0.79	0.82	0.77	0.81	0.76	0.79	0.78	0.78

Figure 13. Although efforts were made to prepare fully homogenous flat glasses, this proved difficult with the compositions of glass used for previous sample preparation. As the redox of the glass would be affected strongly by increasing the temperature to lower the viscosity for amenable pouring, it was decided to incorporate 2-mol% Li₂O into the glass in replacement of Na₂O (see Section 2.1.3). This reduced the high-temperature viscosity of the molten glass through two mechanisms, the mixed alkali effect and reduced connectivity of the silicate network, because of the partial replacement of Na₂O by Li₂O.¹²⁴ However, incorporation of Li₂O also affects the refractive index of the glass by increasing the polarizability of the constituents relative to a glass containing the equivalent quantity of R₂O such as Na₂O or K₂O.¹²⁵

There is an increase in the short-circuit current between the string and module because of lower reflection losses and a minor index matching corresponding to the C-EVA and glass layers. The difference in refractive indices is lower in the module than in the string,

as the C-EVA acts as an index matching layer when bonded together. There are several abbreviations in Table 8 that are explained below.

V_{OC} is the open-circuit voltage, the maximum voltage available from a PV module that occurs at zero current. On the I/V curve shown in Figure 13, this is where the curve touches the x-axis where the y-axis (current) is equal to zero. I_{SC} is the short-circuit current; this is the maximum current available when the voltage across the PV module is zero. On the I/V curve shown in Figure 13, this is where the curve touches the y-axis where the x-axis (voltage) is equal to zero. R_{SERIES} is the series resistance in a PV module. This is a measure of the movement of current across the emitter and base of the module, the resistance across the metal contacts and the silicon (or other PV active material) and the resistance of the top and rear contacts. This results in inefficiencies within the module and reduces the V_{OC} and I_{SC}. R_{SHUNT} is the shunt resistance of a PV module. Low shunt resistance causes power loss in a module as the propagation of the current may follow an alternative path than that designed. Larger values therefore

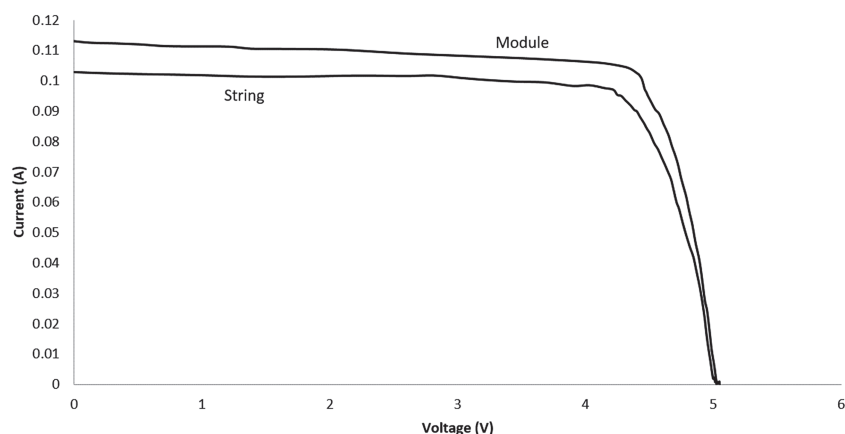
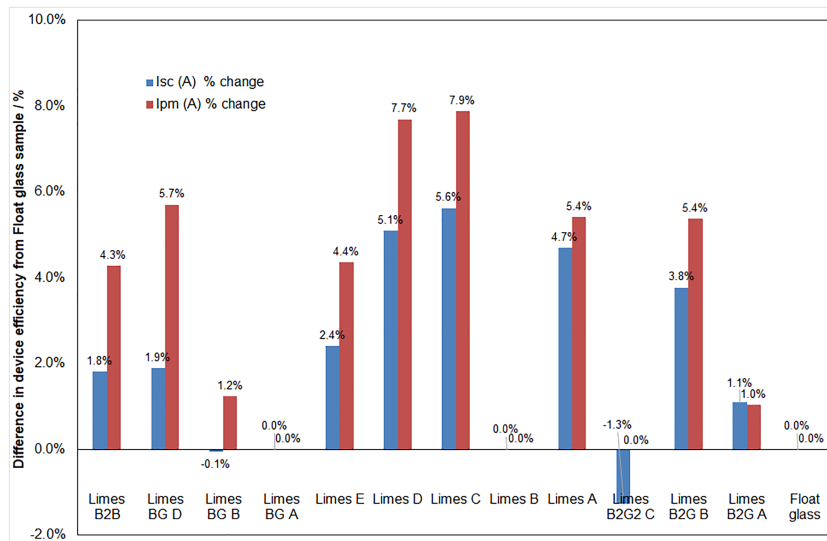


FIGURE 13 Representative measured I/V curve for PV modules prepared at SCT (float glass string and module)

FIGURE 14 Relative enhancement of I_{sc} (blue bars) and I_{pm} (red bars) to float glass [Colour figure can be viewed at wileyonlinelibrary.com]



minimize the difference between theoretical maximum power output and realized power output of a PV module. P_{MAX} is the maximum power (W) of a PV module and is calculated by multiplying the V_{OC} , I_{SC} and fill factor of the module together. V_{PM} is the voltage at maximum power of a PV module, similar to I_{PM} , which is the current at maximum power within a PV module. Fill factor is a measure of the quality of a given PV module and is calculated by dividing the maximum power point by the product of V_{OC} and I_{SC} .

From Tables 8 to 10, the I_{sc} and I_{pm} are shown for each prepared glass and that of a commercially available float glass, and the relative enhancement of the glass is shown in Figure 14. Note that in those

samples, in which the cells have cracked during lamination, the total area available for PV conversion is lowered, and therefore, the relative enhancement appears to be lower. This is an artefact of the broken cells rather than being significantly lower efficiency. In samples without significant damage to the cells, there is an increase in I_{sc} and I_{pm} indicating higher efficiency from the dopants, as illustrated in Figure 14; however, repeated experiments to provide full confirmation of this may be prudent.

It is postulated that the enhancement of the I_{sc} and I_{pm} is due to the addition of fluorescent dopants. The wide variation is due to slight sample differences; not all glasses were able to be prepared to the

TABLE 9 Electrical data for cell strings

		Float	LIMES A	LIMES BG A	LIMES BG B	LIMES BG C	LIMES B2G A	LIMES B2G B	LIMES B2G2	LIMES B2
Property	Uncertainty	Strings								
Irradiance (W/m^2):	± 20	1043	1039	1049	1048	1063	1055	1040	1065	1044
Corrected to (W/m^2):	± 20	1000	1000	1000	1000	1000	1000	1000	1000	1000
Module temp ($^{\circ}C$)	± 1	25.0	24.9	24.6	24.2	24.2	24.5	25.4	25.3	23.8
Corrected to ($^{\circ}C$)	± 1	25	25	25	25	25	25	25	25	25
V_{oc} (V)	± 0.3	5.03	4.96	4.91	4.98	4.98	4.95	5.02	5.03	4.96
I_{sc} (A)	± 0.003	0.102	0.098	0.097	0.100	0.100	0.099	0.102	0.104	0.099
R_{series} (m Ω)	± 10	12.67	8.60	12.86	9.85	8.06	14.66	12.51	11.46	24.19
R_{shunt} (Ω/cm^2)	± 100	2274.31	1403.03	1249.74	1198.94	3304.78	2112.79	1012.15	1869.49	2448.08
P_{max} (W)	± 0.02	0.405	0.381	0.376	0.391	0.394	0.380	0.398	0.405	0.384
V_{pm} (V)	± 0.4	4.22	4.38	4.13	4.18	4.18	4.11	4.19	4.22	4.15
I_{pm} (A)	± 0.005	0.096	0.087	0.091	0.094	0.094	0.093	0.095	0.096	0.093
Fill factor	± 0.05	0.79	0.78	0.79	0.78	0.79	0.78	0.78	0.78	0.78

TABLE 10 Change in I_{sc} and I_{pm} from string to module and damage observations

Property	Float	LIMES A	LIMES BG A	LIMES BG B	LIMES BG C	LIMES B2G A	LIMES B2G B	LIMES B2G2	LIMES B2
I_{sc} (A) % change	9%	−59%	−39%	11%	13%	14%	13%	7%	14%
I_{pm} (A) % change	7%	−68%	−39%	10%	14%	11%	13%	7%	14%
Observations		Cells cracked ×2	Cells cracked ×2	Glass moved				Glass moved	Glass cracked

exact thickness, and slight wedging of all samples was observed. The variable thicknesses give rise to a longer path length, in which photons can be absorbed; however, the increased thickness gives a larger cross-sectional area of fluorescent centres. Thicknesses were however not recorded. Critically all samples demonstrate higher module efficiency. A similar approach carried out by the NREL using CeO_2 as a dopant that absorbed within the UV region and emitted within the visible showed a reduction in the yellowing index after 35 weeks of accelerated ageing testing with UV irradiation.¹¹⁷ A similar effect is proposed to occur within these doped glasses because of the shifted absorbance. Yellowing and ultimately browning of C-EVA has been shown to reduce module efficiency by up to 45% within 5 years of installation,¹²⁶ whereas, as noted in Section 1, the long-term in situ performance of T-EVA in PV modules has not yet been fully investigated—although it is expected to provide superior capabilities to C-EVA, its yellowing index is nonzero,¹⁷ and hence, enhanced protection of T-EVA by the cover glass remains a key requirement.

All doped samples within this study demonstrate an absorbance shifted towards the visible region, of between 2000 and 4000 cm^{-1} (20–40 nm). This shifted absorbance is proposed to increase the service lifetimes of PV modules by reducing the rate of yellowing of C-EVA. As C-EVA comprise some 80% of currently installed c-Si-based PV modules,¹²⁷ and c-Si modules comprise some 87% of all installed capacity of PV modules worldwide,¹²⁸ up to 158 GW of generated PV electricity is affected by yellowing from UV irradiation. Typically, PV module manufacturers expect modules to last between 20 and 25 years, assuming between a 1.0% and 2.5% loss per year.¹²⁹

4 | CONCLUSIONS


SLS glass is ubiquitous for architectural and mobility applications; however, in terms of its application in PV modules, there remains room for improvement. In the current paper, we have reviewed the state of the art and conclude that improvements to PV modules can be made by optimizing the cover glass composition. We have shown that it is possible to increase the CR of cover glass from 0.5 N for conventional SLS float glass to 1.5 N (glass LIMES B) and to increase the chemical resistance by a factor of about 3 as measured using P_{98} (ISO 719). This has been demonstrated for glass compositions that have similar hardness, reduced elastic modulus and thermal properties as for conventional SLS float glass. Iron, when present in float glass,

produces a broad $d-d$ absorption band in the nIR (Fe^{2+}) and narrow $d-d$ bands in the visible (Fe^{3+}), collectively resulting in a significant loss in transmission. However, removal of iron from the glass to increase transmission creates a problem in terms of increased UV transmission, which more rapidly ages the polymeric C-EVA or T-EVA leading to reduced PV module service lifetimes. We have shown here that doping the SLS float glass with Bi_2O_3 and Gd_2O_3 can effectively reduce the UV transmission while keeping the glass essentially free from absorption in the visible and nIR ranges. This is augmented by broad-band down-shifting of absorbed UV photons and re-emission as visible photons available for conversion by the solar cell. The compound effect of these compositional changes to the cover glass thereby enables both increased efficiency and increased lifetime of PV modules. This was also demonstrated for laboratory-scale PV modules in terms of measured I_{sc} and I_{pm} ; however, further measurements to confirm the results are advisable. Thermal strengthening is the predominant technique for providing protection to hailstorms for PV modules; however, this process can be effectively improved in terms of CR by combining with CVD in a one-step process providing a thin film of Al_2O_3 .

ACKNOWLEDGEMENTS

The authors acknowledge with thanks Solar-ERA.NET, the Swedish Energy Agency (contract no. 38349-1) and the Technology Strategy Board (contract no. 620087) for providing funding for this research. We also wish to acknowledge the anonymous reviewers for the detailed review reports that led to significant improvements in our paper.

ORCID

Benjamin L. Allsopp  <https://orcid.org/0000-0002-5828-5083>
Peter Sundberg  <https://orcid.org/0000-0002-8526-8051>
Christina Stålhandske  <https://orcid.org/0000-0002-9173-0847>
Lina Grund  <https://orcid.org/0000-0001-7925-6137>
Anne Andersson  <https://orcid.org/0000-0001-5799-5844>
Paul A. Bingham  <https://orcid.org/0000-0001-6017-0798>
Stefan Karlsson  <https://orcid.org/0000-0003-2160-6979>

REFERENCES

1. IEA, *Solar Energy Perspectives*. IEA Publications. Paris, France: International Energy Agency; 2011.

2. Chapin DM, Fuller CS, Pearson GL. *US Patent 2,780,765*. Bell Telephone Labor Inc; 1957.
3. Timilsina GR, Kurdgelashvili L, Narbel PA. Solar energy: markets, economics and policies. *Renewable and Sustainable Energy Reviews*. 2012;16(1):449-465. <https://doi.org/10.1016/j.rser.2011.08.009>
4. Masson G, Kaizuka I. *Trends in Photovoltaic Applications. Report IEA PVPS T1-36*. IEA Photovoltaic Power Systems Programme 100; 2019.
5. Shah V, Booream-Phelps J. *F.I.T.T. for Investors, Crossing the Chasm, Industry Solar*. Deutsche Bank; 2015.
6. Breyer C, Gerlach A. Global overview on grid-parity. *Progress in Photovoltaics: Research and Applications*. 2013;21(1):121-136. <https://doi.org/10.1002/pip.1254>
7. Ray D. *Lazard's Levelized Cost of Energy Analysis—Version 13.0*. New York, NY, USA: Lazard; 2019:20.
8. Jean J, Brown PR, Jaffe RL, Buonassisi T, Bulovic V. Pathways for solar photovoltaics. *Energy Environ Sci*. 2015;8(4):1200-1219. <https://doi.org/10.1039/c4ee04073b>
9. *International Technology Roadmap for Photovoltaic (ITRPV), in 11th Edition, 2019 Results*. 2020, VDMA Photovoltaic Equipment: itrpv.org.
10. Burrows K, Fthenakis V. Glass needs for a growing photovoltaics industry. *Solar Energy Materials and Solar Cells*. 2015;132:455-459. <https://doi.org/10.1016/j.solmat.2014.09.028>
11. Powell DM, Winkler MT, Choi HJ, Simmons CB, Needleman DB, Buonassisi T. Crystalline silicon photovoltaics: a cost analysis framework for determining technology pathways to reach baseload electricity costs. *Energy Environ Sci*. 2012;5(3):5874-5883. <https://doi.org/10.1039/c2ee03489a>
12. Shou P. The development direction of world flat glass and energy conservation and environment protection. *Glass Physics and Chemistry*. 2015;41(1):1-8. <https://doi.org/10.1134/s1087659615010198>
13. Rühle S. Tabulated values of the Shockley-Queisser limit for single junction solar cells. *Solar Energy*. 2016;130:139-147. <https://doi.org/10.1016/j.solener.2016.02.015>
14. Green MA, Hishikawa Y, Warta W, et al. Solar cell efficiency tables (version 50). *Progress in Photovoltaics: Research and Applications*. 2017;25(7):668-676. <https://doi.org/10.1002/pip.2909>
15. Kuitche JM, Pan R, Tamizhmani G. Investigation of dominant failure mode(s) for field-aged crystalline silicon PV modules under desert climatic conditions. *IEEE Journal of Photovoltaics*. 2014;4(3):814-826. <https://doi.org/10.1109/JPHOTOV.2014.2308720>
16. Vogt MR, Holst H, Schulte-Huxel H, et al. Optical constants of UV transparent EVA and the impact on the PV module output power under realistic irradiation. *Energy Procedia*. 2016;92:523-530. <https://doi.org/10.1016/j.egypro.2016.07.136>
17. Adothu B, Chattopadhyay S, Bhatt P, Hui P, Costa FR, Mallick S. *Early-Stage Identification of Encapsulants Photobleaching and Discoloration in Crystalline Silicon Photovoltaic Module Laminates*. Progress in Photovoltaics: Research and Applications. DOI: <https://doi.org/10.1002/pip.3269>
18. Thomsen SV, Landa KA, Hulme R, Longobardo AV, Landa L, Broughton A. *US Patent 7,557,053*. Guardian Industries Corp; 2010.
19. Donald SB, Swink AM, Schreiber HD. High-iron ferric glass. *Journal of Non-Crystalline Solids*. 2006;352(6-7):539-543. <https://doi.org/10.1016/j.jnoncrysol.2005.11.042>
20. Atkarskaya AB, Bykov VN. Clarification of glass using arsenic and antimony oxides. *Glass and Ceramics*. 2003;60(11):389-391. <https://doi.org/10.1023/b:glac.0000020796.91900.46>
21. Deubener J, Hensch G, Moiseev A, Bornhöft H. Glasses for solar energy conversion systems. *Journal of the European Ceramic Society*. 2009;29(7):1203-1210. <https://doi.org/10.1016/j.jeurceramsoc.2008.08.009>
22. Campbell P, Green MA. Light trapping properties of pyramidally textured surfaces. *Journal of Applied Physics*. 1987;62(1):243-249. <https://doi.org/10.1063/1.339189>
23. Müller J, Rech B, Springer J, Vanecek M. TCO and light trapping in silicon thin film solar cells. *Solar Energy*. 2004;77(6):917-930. <https://doi.org/10.1016/j.solener.2004.03.015>
24. Nielsen KH, Orzol DK, Koynov S, Carney S, Hultstein E, Wondraczek L. Large area, low cost anti-reflective coating for solar glasses. *Solar Energy Materials and Solar Cells*. 2014;128(0):283-288. <https://doi.org/10.1016/j.solmat.2014.05.034>
25. Jorgensen G, Brunold S, Köhl M, Nostell P, Oversloot H, Roos A. *Durability Testing of Antireflection Coatings for Solar Applications, in SPIE's 44th Annual Meeting and Exhibition*. Denver, USA; 1999.
26. Gombert A, Glauert W, Rose K, et al. Antireflective transparent covers for solar devices. *Solar Energy*. 2000;68(4):357-360. [https://doi.org/10.1016/S0038-092X\(00\)00022-0](https://doi.org/10.1016/S0038-092X(00)00022-0)
27. Brow RK, Schmitt ML. A survey of energy and environmental applications of glass. *Journal of the European Ceramic Society*. 2009;29(7):1193-1201. <https://doi.org/10.1016/j.jeurceramsoc.2008.08.011>
28. Shelby JE, Vitko J Jr, Pantano CG. Weathering of glasses for solar applications. *Solar Energy Materials*. 1980;3(1-2):97-110. [https://doi.org/10.1016/0165-1633\(80\)90052-0](https://doi.org/10.1016/0165-1633(80)90052-0)
29. Osterwald CR, Benner JP, Pruett J, Anderberg A, Rummel S, Ottoson L. Degradation in weathered crystalline-silicon PV modules apparently caused by UV radiation. In: *3rd World Conference on Photovoltaic Energy Conversion*. Osaka, Japan; 2003.
30. Jordan DC, Kurtz SR. Photovoltaic degradation rates—an analytical review. *Progress in Photovoltaics: Research and Applications*. 2013; 21(1):12-29. <https://doi.org/10.1002/pip.1182>
31. Jordan D, Kurtz S. 3—Photovoltaic module stability and reliability A2. In: Pearsall N, ed. *The Performance of Photovoltaic (PV) Systems*. Woodhead Publishing; 2017:71-101.
32. Jentsch A, Eichhorn KJ, Voit B. Influence of typical stabilizers on the aging behavior of EVA foils for photovoltaic applications during artificial UV-weathering. *Polymer Testing*. 2015;44:242-247. <https://doi.org/10.1016/j.polymertesting.2015.03.022>
33. Shamachurn H, Betts T. Experimental study of the degradation of silicon photovoltaic devices under ultraviolet radiation exposure. *Journal of Solar Energy*. 2016;2016(9):2473245. <https://doi.org/10.1155/2016/2473245>
34. Volotinen TT, Parker JM, Bingham PA. Concentrations and site partitioning of Fe²⁺ and Fe³⁺ ions in a soda-lime-silica glass obtained by optical absorbance spectroscopy. *Physics and Chemistry of Glasses - European Journal of Glass Science and Technology Part B*. 2008;49(5):258-270.
35. Vogt MR, Hahn H, Holst H, et al. Measurement of the optical constants of soda-lime glasses in dependence of iron content and modeling of iron-related power losses in crystalline Si solar cell modules. *IEEE Journal of Photovoltaics*. 2016;6(1):111-118. <https://doi.org/10.1109/JPHOTOV.2015.2498043>
36. Wondraczek L, Tyystjärvi E, Méndez-Ramos J, Müller FA, Zhang Q. Shifting the sun: solar spectral conversion and extrinsic sensitization in natural and artificial photosynthesis. *Advanced Science*. 2015; 2(12):1500218. <https://doi.org/10.1002/advs.201500218>
37. Day J, Senthilarasu S, Mallick TK. Improving spectral modification for applications in solar cells: a review. *Renewable Energy*. 2019;132:186-205. <https://doi.org/10.1016/j.renene.2018.07.101>
38. Levitt JA, Weber WH. Materials for luminescent greenhouse solar collectors. *Appl Optics*. 1977;16(10):2684-2689.
39. Weber WH, Lambe J. Luminescent greenhouse collector for solar radiation. *Appl Optics*. 1976;15(10):2299-2300. <https://doi.org/10.1364/ao.15.002299>
40. Reisfeld R, Neuman S. Planar solar energy converter and concentrator based on uranyl-doped glass. *Nature*. 1978;274(5667):144-145.
41. Reisfeld R, Kalisky Y. Improved planar solar converter based on uranyl neodymium and holmium glasses. *Nature*. 1980;283(5744):281-282.

42. Strümpel C, McCann M, Beaucarne G, et al. Modifying the solar spectrum to enhance silicon solar cell efficiency—an overview of available materials. *Solar Energy Materials and Solar Cells*. 2007;91(4): 238–249. <https://doi.org/10.1016/j.solmat.2006.09.003>
43. Huang X, Han S, Huang W, Liu X. Enhancing solar cell efficiency: the search for luminescent materials as spectral converters. *Chem Soc Rev*. 2013;42(1):173–201. <https://doi.org/10.1039/c2cs35288e>
44. Trupke T, Green MA, Würfel P. Improving solar cell efficiencies by down-conversion of high-energy photons. *Journal of Applied Physics*. 2002;92(3):1668–1674. <https://doi.org/10.1063/1.1492021>
45. Richards BS. Luminescent layers for enhanced silicon solar cell performance: down-conversion. *Solar Energy Materials and Solar Cells*. 2006; 90(9):1189–1207. <https://doi.org/10.1016/j.solmat.2005.07.001>
46. Dejneka MJ, Streltsov A, Pal S, et al. Rare earth-doped glass micro-barcode. *Proc Natl Acad Sci*. 2003;100(2):389–393. <https://doi.org/10.1073/pnas.0236044100>
47. van der Ende BM, Aarts L, Meijerink A. Lanthanide ions as spectral converters for solar cells. *Phys Chem Chem Phys*. 2009;11(47): 11081–11095. <https://doi.org/10.1039/b913877c>
48. Reisfeld R. Fluorescent dyes in sol-gel glasses. *J Fluoresc*. 2002; 12(3):317–325. <https://doi.org/10.1023/a:1021397422976>
49. Molkenova A, Khamkhash L, Zhussupbekova A, et al. Solution-based deposition of transparent Eu-doped titanium oxide thin films for potential security labeling and UV screening. *Nanomaterials*. 2020; 10(6):1132. <https://doi.org/10.3390/nano10061132>
50. Johansson W, Peralta A, Jonson B, Anand S, Österlund L, Karlsson S. Transparent TiO₂ and ZnO thin films on glass for UV protection of PV modules. *Frontiers in Materials*. 2019;6(259):1–10. <https://doi.org/10.3389/fmats.2019.00259>
51. van Sark W, Meijerink A, Schropp R. Solar spectrum conversion for photovoltaics using nanoparticles. In: Fthenakis V, ed. *Third Generation Photovoltaics CIER-E-2012-8*. InTech; 2012:1–28.
52. Cattaruzza E, Mardegan M, Pregolato T, et al. Ion exchange doping of solar cell coverglass for sunlight down-shifting. *Solar Energy Materials and Solar Cells*. 2014;130(0):272–280. <https://doi.org/10.1016/j.solmat.2014.07.028>
53. Ali S, Iqbal Y, Ajmal M, Gonella F, Cattaruzza E, Quaranta A. Field-driven diffusion of transition metal and rare-earth ions in silicate glasses. *Journal of Non-Crystalline Solids*. 2014;405(0):39–44. <https://doi.org/10.1016/j.jnoncrysol.2014.08.042>
54. Debije MG, Verbunt PPC. Thirty years of luminescent solar concentrator research: solar energy for the built environment. *Advanced Energy Materials*. 2012;2(1):12–35. <https://doi.org/10.1002/aenm.201100554>
55. Neuroth, N, Haspel R. Glasses for luminescent solar concentrators. 1986: p. 88–92. <https://doi.org/10.1117/12.938313>
56. Reisfeld R. New developments in luminescence for solar energy utilization. *Optical Materials*. 2010;32(9):850–856. <https://doi.org/10.1016/j.optmat.2010.04.034>
57. Weyl WA. *Coloured Glasses*. 2nd ed. Sheffield: Society of Glass Technology; 1967.
58. Burns RG. *Mineralogical Applications of Crystal Field Theory*. Mineralogical Applications of Crystal Field Theory. 575 Cambridge, UK: Cambridge University Press; 1993.
59. Keppler H. Crystal field spectra and geochemistry of transition metal ions in silicate melts and glasses. *Am Mineral*. 1992;77(1–2):62–75.
60. Bates T. Ligand field theory and absorption spectra of transition-metal ions in glasses. In: Mackenzie JD, ed. *Modern aspects of the vitreous state*. London: Butterworths; 1962:195–254.
61. Peng M, Wondraczek L. Bismuth-doped oxide glasses as potential solar spectral converters and concentrators. *J Mater Chem*. 2009; 19(5):627–630.
62. Xu W, Peng M, Ma Z, Dong G, Qiu J. A new study on bismuth doped oxide glasses. *Opt Express*. 2012;20(14):15692–15702. <https://doi.org/10.1364/oe.20.015692>
63. Allsopp, BL, Christopoulou G, Brookfield A, Forder SD, Bingham PA. Optical and structural properties of d 0 ion-doped silicate glasses for photovoltaic applications. *Physics and Chemistry of Glasses—European Journal of Glass Science and Technology Part B*. 2018. 59(4): p. 193–202. <https://doi.org/10.13036/17533562.59.4.003>
64. Allsopp, BL, Bingham PA, Booth J, Johnson SR, Orman R. Composition and device, UK Patent Application GB2553163. 2018.
65. Chen T.-Y., Rautiyal P., Vaishnav S., et al. Composition-structure-property effects of antimony in soda-lime-silica glasses. *J Non-Cryst Solids*. 2020;544:120184. <https://doi.org/10.1016/j.jnoncrysol.2020.120184>
66. Goldschmidt JC, Fischer S. Upconversion for photovoltaics—a review of materials, devices and concepts for performance enhancement. *Advanced Optical Materials*. 2015;3(4):510–535. <https://doi.org/10.1002/adom.201500024>
67. Shalav A, Richards BS, Green MA. Luminescent layers for enhanced silicon solar cell performance: up-conversion. *Solar Energy Materials and Solar Cells*. 2007;91(9):829–842. <https://doi.org/10.1016/j.solmat.2007.02.007>
68. Auzel F. Upconversion and anti-stokes processes with f and d ions in solids. *Chem Rev*. 2004;104(1):139–174. <https://doi.org/10.1021/cr020357g>
69. Wondraczek L, Mauro JC, Eckert J, et al. Towards ultrastrong glasses. *Adv Mater*. 2011;23(39):4578–4586. <https://doi.org/10.1002/adma.201102795>
70. Irwin G. Analysis of stresses and strains near the end of a crack traversing a plate. *J Appl Mech*. 1957;24:361–364.
71. Hand RJ. Mechanical properties of glass. In: Richet P, ed. *Encyclopedia for Glass Science, Technology, History and Culture*. Hoboken, NJ: John Wiley & Sons Inc.; 2019.
72. Gardon R. Thermal tempering of glass. In: Uhlmann DR, Kreidl NJ, eds. *Glass Science and Technology vol 5 Elasticity and Strength in Glasses*. New York: Academic Press; 1980:145–216.
73. Narayanaswamy OS, Gardon R. Calculation of residual stresses in glass. *J Am Ceram Soc*. 1969;52(10):554–558. <https://doi.org/10.1111/j.1151-2916.1969.tb09163.x>
74. Karlsson S, Wondraczek L. Strengthening of oxide glasses. In: Richet P, ed. *Encyclopedia for Glass Science, Technology, History and Culture*. Hoboken, NJ: John Wiley & Sons Inc.; 2020.
75. Karlsson S, Jonson B, Stålhandske C. The technology of chemical glass strengthening—a review. *Glass Technology—European Journal of Glass Science and Technology Part A*. 2010;51(2):41–54.
76. Fluegel A. Thermal expansion calculation for silicate glasses at 210°C based on a systematic analysis of global databases. *Glass Technology - European Journal of Glass Science and Technology Part A*. 2010;51(5):191–201.
77. Kasper A, Yousfi O. Spontaneous glass breakage caused by nickel sulphide (a review). In: *Proceedings of Glass Performance Days (GPD)*. Finland: Tampere; 2009.
78. Karlsson, S., *Spontaneous Fracture in Thermally Strengthened Glass—A Review and Outlook*. *Ceramics-Silikáty*, 2017;61(3):188–201. <https://doi.org/10.13168/cs.2017.0016>
79. Gulati S, Roe T, Vitkala J. Importance of edge finish on thermal tempering. In: *Conference Proceedings, Glass Processing Days*. Finland: Tampere; 2001 Glassfiles.com.
80. Mognato E, Schiavonato M, Barbieri A, Pittoni M. Process influences on mechanical strength of chemical strengthened glass. *Glass Structures & Engineering*. 2016;1–14. <https://doi.org/10.1007/s40940-016-0019-0>
81. Gy, R., Ion exchange for glass strengthening. *Materials science & engineering. B, Solid-state materials for advanced technology*, 2008. 149(2): p. 159. DOI: <https://doi.org/10.1016/j.mseb.2007.11.029>
82. Varshneya AK. The Physics of chemical strengthening of glass: room for a new view. *Journal of Non-Crystalline Solids*. 2010;356(44–49): 2289–2294. <https://doi.org/10.1016/j.jnoncrysol.2010.05.010>

83. Varshneya AK. Chemical strengthening of glass: lessons learned and yet to be learned. *International Journal of Applied Glass Science*. 2010; 1(2):131-142. <https://doi.org/10.1111/j.2041-1294.2010.00010.x>
84. Varshneya AK, Kreski PK. The chemistry of chemical strengthening of glass. In: *Processing, Properties, and Applications of Glass and Optical Materials*. John Wiley & Sons, Inc; 2012:107-114.
85. Wang HF, Xing GZ, Wang XY, Zhang LL, Zhang L, Li S. Chemically strengthened protection glasses for the applications of space solar cells. *AIP Advances*. 2014;4(4):1-7. <https://doi.org/10.1063/1.4873538>
86. Kambe M, Hara K, Mitarai K, et al. Chemically strengthened cover glass for preventing potential induced degradation of crystalline silicon solar cells. In: *2013 IEEE 39th Photovoltaic Specialists Conference (PVSC)*; 2013.
87. Griffith AA. The phenomena of rupture and flow in solids. *Philosophical Transactions of the Royal Society of London—Series A, Containing Papers of a Mathematical or Physical Character*. 1921;221:163-198.
88. Hasdemir I, Striepe S, Deubener J, Simon K. A 2000-year perspective on indentation crack resistance and brittleness of glass. *Journal of Non-Crystalline Solids*. 2015;408(0):51-56. <https://doi.org/10.1016/j.jnoncrysol.2014.10.012>
89. Sehgal J, Ito S. Brittleness of glass. *Journal of Non-Crystalline Solids*. 1999;253(1-3):126-132. [https://doi.org/10.1016/S0022-3093\(99\)00348-8](https://doi.org/10.1016/S0022-3093(99)00348-8)
90. Lawn BR, Marshall DB. Hardness, toughness, and brittleness: an indentation analysis. *J am Ceram Soc*. 1979;62(7-8):347-350. <https://doi.org/10.1111/j.1151-2916.1979.tb19075.x>
91. Hand RJ, Tadjiev DR. Mechanical properties of silicate glasses as a function of composition. *J Non Cryst Solids*. 2010;356(44-49):2417-2423.
92. Sehgal J, Ito S. A new low-brittleness glass in the soda-lime-silica glass family. *J am Ceram Soc*. 1998;81(9):2485-2488. <https://doi.org/10.1111/j.1151-2916.1998.tb02649.x>
93. Rouxel T, Sellappan P, Célarié F, Houizot P, Sanglebœuf J-C. Toward glasses with better indentation cracking resistance. *Comptes Rendus Mécanique*. 2014;342(1):46-51. <https://doi.org/10.1016/j.crme.2013.10.008>
94. Sellappan P, Rouxel T, Celarie F, Becker E, Houizot P, Conradt R. Composition dependence of indentation deformation and indentation cracking in glass. *Acta Materialia*. 2013;61(16):5949-5965. <https://doi.org/10.1016/j.actamat.2013.06.034>
95. Kilinc E, Hand RJ. Mechanical properties of soda-lime-silica glasses with varying alkaline earth contents. *Journal of non-crystalline solids*. 2015;429:190-197. <https://doi.org/10.1016/j.jnoncrysol.2015.08.013>
96. Tadjiev DR, Hand RJ. Inter-relationships between composition and near surface mechanical properties of silicate glasses. *Journal of Non-Crystalline Solids*. 2008;354(47-51):5108-5109. <https://doi.org/10.1016/j.jnoncrysol.2008.05.080>
97. Sundberg P, Grund Bäck L, Orman R, Booth J, Karlsson S. Simultaneous chemical vapor deposition and thermal strengthening of glass. *Thin Solid Films*. 2019;669:487-493. <https://doi.org/10.1016/j.tsf.2018.11.028>
98. Baquedano E, Torné L, Caño P, Postigo P. Increased efficiency of solar cells protected by hydrophobic and hydrophilic anti-reflecting nanostructured glasses. *Nanomaterials*. 2017;7(12):437. <https://doi.org/10.3390/nano7120437>
99. Baquedano E, Martinez R, Llorens J, Postigo P. Fabrication of silicon nanobelts and nanopillars by soft lithography for hydrophobic and hydrophilic photonic surfaces. *Nanomaterials*. 2017;7(5):109. <https://doi.org/10.3390/nano7050109>
100. Wallenberger FT, Bingham PA. *Fiberglass and Glass Technology: Energy-Friendly Compositions*. Springer; 2010.
101. Fluegel A. Global model for calculating room-temperature glass density from the composition. *J am Ceram Soc*. 2007;90(8):2622-2625. <https://doi.org/10.1111/j.1551-2916.2007.01751.x>
102. Quinn GD, Bradt RC. On the Vickers indentation fracture toughness test. *J am Ceram Soc*. 2007;90(3):673-680. <https://doi.org/10.1111/j.1551-2916.2006.01482.x>
103. Kato Y, Yamazaki H, Yoshida S, Matsuoka J. Effect of densification on crack initiation under Vickers indentation test. *Journal of Non-Crystalline Solids*. 2010;356(35-36):1768-1773. <https://doi.org/10.1016/j.jnoncrysol.2010.07.015>
104. Limbach R, Karlsson S, Scannell G, Mathew R, Edén M, Wondraczek L. The effect of TiO₂ on the structure of Na₂O-CaO-SiO₂ glasses and its implications for thermal and mechanical properties. *Journal of Non-Crystalline Solids*. 2017;471:6-18. <https://doi.org/10.1016/j.jnoncrysol.2017.04.013>
105. Lakatos T, Johansson L, Simmingsköld B. The effect of some glass components on the viscosity of glass. *Glasteknisk Tidskrift*. 1972;27(2):25-28.
106. ISO 9845-1:1992, Solar energy—Reference solar spectral irradiance at the ground at different receiving conditions—Part 1: Direct normal and hemispherical solar irradiance for air mass 1.5.
107. Reiß S, Krischok S, Rädlein E. Comparative study of weather induced corrosion mechanisms of toughened and normal float glasses. *Glass Technology—European Journal of Glass Science and Technology Part A*. 2019;60(2):33-44. <https://doi.org/10.13036/17533546.60.2.020>
108. Lyle AK. Theoretical aspects of chemical attack of glasses by water*. *J am Ceram Soc*. 1943;26(6):201-204. <https://doi.org/10.1111/j.1151-2916.1943.tb15211.x>
109. Richardson RM, Dalgliesh RM, Brennan T, Lovell MR, Barnes AC. A neutron reflection study of the effect of water on the surface of float glass. *Journal of Non-Crystalline Solids*. 2001. 292(1): p. 93-107. DOI: [https://doi.org/10.1016/S0022-3093\(01\)00885-7](https://doi.org/10.1016/S0022-3093(01)00885-7)
110. Wassick TA, Doremus RH, Lanford WA, Burman C. Hydration of soda-lime silicate glass, effect of alumina. *Journal of Non-Crystalline Solids*. 1983;54(1-2):139-151. [https://doi.org/10.1016/0022-3093\(83\)90088-1](https://doi.org/10.1016/0022-3093(83)90088-1)
111. El-Batal FH, Khalil EM, Hamdy YM, Zidan HM, Aziz MS, Abdelghany AM. FTIR spectral analysis of corrosion mechanisms in soda lime silica glasses doped with transition metal oxides. *Silicon*. 2010;2(1):41-47. <https://doi.org/10.1007/s12633-010-9037-8>
112. Koenderink GH, Brzesowsky RH, Balkenende AR. Effect of the initial stages of leaching on the surface of alkaline earth sodium silicate glasses. *Journal of Non-Crystalline Solids*. 2000. 262(1): p. 80-98. DOI: [https://doi.org/10.1016/S0022-3093\(99\)00704-8](https://doi.org/10.1016/S0022-3093(99)00704-8)
113. Wang M, Cheng J, Liu Q, Tian P, Li M. The effect of light rare earths on the chemical durability and weathering of Na₂O-CaO-SiO₂ glasses. *Journal of Nuclear Materials*. 2010;400(2):107-111. <https://doi.org/10.1016/j.jnucmat.2010.02.018>
114. Guillemet C. Annealing and tempering of glass. *Journal of Non-Crystalline Solids*. 1990;123(1-3):415-426. [https://doi.org/10.1016/0022-3093\(90\)90813-2](https://doi.org/10.1016/0022-3093(90)90813-2)
115. Yang J, Lee D, Baek D, Kim D, Nam J, Huh P. Effect of various encapsulants for frameless glass to glass Cu (In,Ga)(Se,S)₂ photovoltaic module. *RSC Adv*. 2015;5(63):51258-51262. <https://doi.org/10.1039/C5RA03663A>
116. Fix T, Nona TA, Imbert D, et al. Enhancement of silicon solar cells by downshifting with Eu and Tb coordination complexes. *Progress in Photovoltaics: Research and Applications*. 2016;24(9):1251-1260. <https://doi.org/10.1002/pip.2785>
117. Holley W Jr, Agro S, Galica J, Yorgensen R. *Advanced EVA-based encapsulants*. NCPV FY 1998 Annual Report; 1998:377.
118. Wang Z, Cheng L. Effects of doping CeO₂/TiO₂ on structure and properties of silicate glass. *Journal of Alloys and Compounds*. 2014; 597:167-174. <https://doi.org/10.1016/j.jallcom.2014.01.232>
119. Holley WW, Agro SC. *Advanced EVA-Based Encapsulants*, in NREL/SR-520-25296. Enfield, Connecticut; 1998.
120. Fujimoto Y. Local structure of the infrared bismuth luminescent center in Bismuth-doped silica glass. *J am Ceram Soc*. 2010;93(2):581-589. <https://doi.org/10.1111/j.1551-2916.2009.03419.x>

121. Boulon, G, Moine B, Bourcet JC, Reifel R, Kalisky Y. Time resolved spectroscopy about 3P1 and 3P0 levels in Bi3+ doped germanate glasses. *Journal of luminescence*, 1979;18-19:924-928. [https://doi.org/10.1016/0022-2313\(79\)90265-5](https://doi.org/10.1016/0022-2313(79)90265-5).
122. Shifeng Z, Nan J, Bin Z, et al. Multifunctional bismuth-doped nanoporous silica glass: from blue-green, orange, red, and white light sources to ultra-broadband infrared amplifiers. *Adv Funct Mater*. 2008;18(9):1407-1413. <https://doi.org/10.1002/adfm.200701290>
123. Pisano G, Carfagni GR. Statistical interference of material strength and surface prestress in heat-treated glass. *J am Ceram Soc*. 2017; 100(3):954-967. <https://doi.org/10.1111/jace.14608>
124. Wright BM, Shelby JE. Phase separation and the mixed alkali effect. *Phys Chem Glasses*. 2000;41(4):192-198.
125. Duffy JA. Ultraviolet transparency of glass: a chemical approach in terms of band theory, polarisability and electronegativity. *Phys Chem Glasses*. 2001;42(3):151-157.
126. Pern FJ. Ethylene-vinyl acetate (EVA) encapsulants for photovoltaic modules: degradation and discoloration mechanisms and formulation modifications for improved photostability. *Die Angewandte Makromolekulare Chemie*. 1997;252(1):195-216. <https://doi.org/10.1002/apmc.1997.052520114>
127. Jiang S, Wang K, Zhang H, Ding Y, Yu Q. Encapsulation of PV modules using ethylene vinyl acetate copolymer as the encapsulant. *Macromolecular Reaction Engineering*. 2015;9(5):522-529. <https://doi.org/10.1002/mren.201400065>
128. Ch. 8: Solar. In: *World Energy Resources*. London, United Kingdom: World Energy Council; 2016.
129. Czanderna AW, Jorgensen GJ. Service lifetime prediction for encapsulated photovoltaic cells/minimodules. *AIP Conference Proceedings*. 1997;394(1):295-312. <https://doi.org/10.1063/1.52899>

How to cite this article: Allsopp BL, Orman R, Johnson SR, et al. Towards improved cover glasses for photovoltaic devices. *Prog Photovolt Res Appl*. 2020;1–20. <https://doi.org/10.1002/pip.3334>